

# Observational and model evidence for a prominent stratospheric influence on variability in tropospheric nitrous oxide

Cynthia D. Nevison<sup>1</sup>, Qing Liang<sup>2</sup>, Paul A. Newman<sup>2</sup>, Britton B. Stephens<sup>3</sup>, Geoff Dutton<sup>4,5</sup>, Xin Lan<sup>4,5</sup>,  
Roisin Commane<sup>6</sup>, Yenny Gonzalez<sup>7,8</sup>, Eric Kort<sup>9</sup>

<sup>1</sup>Institute for Arctic and Alpine Research, University of Colorado, Boulder, CO, USA

<sup>2</sup>NASA Goddard Space Flight Center, Greenbelt, MD, USA

<sup>3</sup>NSF National Center for Atmospheric Research, Boulder, CO, USA

<sup>4</sup>Global Monitoring Laboratory, NOAA Earth System Research Laboratory, Boulder, CO, USA

<sup>5</sup>Cooperative Institute for Research in Environmental Sciences (CIRES), University of Colorado, Boulder, CO, USA

<sup>6</sup>Department of Earth & Environmental Sciences, Lamont-Doherty Earth Observatory, Columbia University, Palisades, NY, USA

<sup>7</sup>CIMEL Electronique, Paris, 75011, France

<sup>8</sup>Izaña Atmospheric Research Center, AEMET, Santa Cruz de Tenerife, 38001, Spain

<sup>9</sup>Department of Climate & Space Sciences & Engineering, University of Michigan, Ann Arbor, MI, USA

Correspondence to: Cynthia D. Nevison (cynthia.nevison@colorado.edu)

## Abstract

The literature presents different views on how the stratosphere influences variability in surface nitrous oxide (N<sub>2</sub>O) and on whether that influence is outweighed by surface emission changes driven by the El Niño Southern Oscillation (ENSO). These questions are investigated using a chemistry-climate model with a stratospheric N<sub>2</sub>O tracer, surface and aircraft-based N<sub>2</sub>O measurements, and indices for ENSO, polar lower stratospheric temperature (PLST), and the stratospheric quasi-biennial oscillation (QBO). The model simulates well-defined seasonal cycles in tropospheric N<sub>2</sub>O that are caused mainly by the seasonal descent of N<sub>2</sub>O-poor stratospheric air in polar regions with subsequent cross-tropopause transport and mixing. Similar seasonal cycles are identified in recently available N<sub>2</sub>O data from aircraft. A correlation analysis between the N<sub>2</sub>O atmospheric growth rate (AGR) anomaly in long-term surface monitoring data and the ENSO, PLST, and QBO indices reveals hemispheric differences. In the northern hemisphere, the surface N<sub>2</sub>O AGR is negatively correlated with winter (January-March) PLST. This correlation is consistent with an influence from the Brewer Dobson Circulation, which brings N<sub>2</sub>O-poor air from the middle and upper stratosphere into the lower stratosphere, with associated warming due to diabatic descent. In the southern hemisphere, the N<sub>2</sub>O AGR is better correlated to QBO and ENSO indices. These different hemispheric influences on the N<sub>2</sub>O AGR are consistent with known

Deleted: ¶

Deleted: v

Deleted: ¶

Deleted: ing

Deleted: variability in

Deleted: is influenced by the stratosphere and

Deleted: forcings

Deleted: associated with

Deleted: outweigh those influences

Deleted: These issues are relevant to interpreting biogeochemical source signals in

Deleted: tropospheric N<sub>2</sub>O

Deleted: and are

Deleted: here

Deleted: surface and aircraft-based atmospheric N<sub>2</sub>O measurements and ...

Deleted: .

Deleted: predominantly

Formatted: Subscript

Deleted: global airborne surveys and aircraft-based monitoring

Deleted: the annually averaged

Deleted: atmospheric growth rate anomaly derived from long-term monitoring data

Deleted: polar lower stratospheric temperature

Deleted: c

Deleted: warm,

Deleted: atmospheric growth rate

Deleted: anomaly

Deleted: indices of ENSO and the stratospheric quasi-biennial oscillation (QBO)

Deleted: differences

Deleted: in the factors influencing

Deleted: growth rate

atmospheric dynamics and the complex interaction of the QBO with the Brewer Dobson Circulation.  
More airborne surveys, extending to the tropopause, would help elucidate the stratospheric influence on  
tropospheric N<sub>2</sub>O, allowing for better understanding of surface sources.

**Deleted:** circulation

**Deleted:** , which provide high-resolution N<sub>2</sub>O data near

**Deleted:** refine our understanding of

**Deleted:** the

**Deleted:** e

**Deleted:** and enhance our ability t

**Deleted:** o interpret

**Deleted:** N<sub>2</sub>O

**Deleted:** ¶

**Formatted:** Subscript

**Deleted:**

**Formatted:** Font: Bold

**Formatted:** Font: Bold

**Formatted:** Normal, Don't adjust right indent when grid is defined, Line spacing: 1.5 lines, No widow/orphan control, Don't adjust space between Latin and Asian text, Don't adjust space between Asian text and numbers

**Deleted:** an important ozone-depleting substance and

**Deleted:** ,

**Deleted:** (GWP)

**Deleted:** N

**Deleted:**

**Deleted:** nitrogen (N)

**Deleted:** While 1

## 70 **1. Introduction**

Nitrous oxide (N<sub>2</sub>O) is a long-lived greenhouse gas with a global warming potential of 265 relative to CO<sub>2</sub> over a 100 year time horizon (*WMO*, 2018). N<sub>2</sub>O has an atmospheric lifetime of about 120 years and is destroyed slowly in the stratosphere by both photolysis and oxidation, with a fraction of the oxidation product yielding NO<sub>x</sub>, a catalyst of stratospheric ozone destruction (*Crutzen*, 1970;  
75 *Ravishankara et al.*, 2009; *Prather et al.*, 2015). N<sub>2</sub>O has abundant natural microbial sources in soil, freshwater and oceans, which account for the majority of global emissions, although anthropogenic sources are becoming increasingly important (*Tian et al.*, 2020; *Canadell et al.*, 2021).

The atmospheric N<sub>2</sub>O concentration has risen from about ~270 ppb preindustrially to 336 ppb by 2022  
80 (*MacFarling-Meure et al.*, 2006; *Lan et al.*, 2022). This rise has been attributed largely to Haber-Bosch industrial nitrogen (N), fixation to produce agricultural fertilizer, which has increased the substrate available to N-cycling microbes (*Park et al.*, 2012). Recent evidence suggests that N<sub>2</sub>O is increasing at an accelerating rate in the atmosphere, possibly due to a nonlinear response of microbes to increasing N inputs in intensively fertilized agricultural systems (*Thompson et al.*, 2019; *Liang et al.*, 2022).

85 High precision measurements of N<sub>2</sub>O have revealed interannual variability in its atmospheric growth rate (AGR) and small-amplitude seasonal cycles in the range of 0.4 to 1 ppb (*Nevison et al.*, 2004; 2007; 2011; *Jiang et al.*, 2007; *Thompson et al.*, 2013). Spatial gradients in atmospheric N<sub>2</sub>O are also small, e.g., the northern hemisphere (NH) minus southern hemisphere (SH) difference is approximately 1 ppb  
90 (*Thompson et al.*, 2014b; *Liang et al.*, 2022). Larger spatial and seasonal signals in atmospheric N<sub>2</sub>O have been observed at sites influenced by strong local agricultural or coastal upwelling sources (*Lueker et al.*, 2003; *Nevison et al.*, 2018; *Ganesan et al.*, 2020). However, at sites remote from local sources

110 even variations of 0.2 ppb in estimated background N<sub>2</sub>O levels can significantly affect the magnitude of  
N<sub>2</sub>O emissions inferred from atmospheric inversions (Nevison *et al.*, 2018).

A few studies have inferred information about surface biogeochemical sources based on the observed  
seasonal cycle in atmospheric N<sub>2</sub>O at remote monitoring sites. However, these studies have cautioned  
115 that the transport of N<sub>2</sub>O-poor air from the stratosphere is a major cause of both seasonal and  
interannual variability in surface N<sub>2</sub>O, which complicates the interpretation of surface emission signals  
(Nevison *et al.*, 2005; 2011; 2012; Thompson *et al.*, 2014b; Ray *et al.*, 2020; Ruiz *et al.*, 2021). Other  
studies have argued that ENSO cycles are the major driver of interannual variability in tropospheric  
N<sub>2</sub>O (Ishijima *et al.*, 2009; Thompson *et al.*, 2013; Canadell *et al.*, 2021) or that ENSO-driven  
120 variability can obscure the influence of the stratosphere in some years (Ruiz *et al.*, 2021). ENSO refers  
to the periodic oscillation between warm (El Niño) and cold (La Niña) phases in [sea surface  
temperature over](#) the eastern tropical Pacific (ETP). During the El Niño phase, the warming and  
deepening of the thermocline is associated with reduced upwelling in the ETP and drought in South  
America, which can decrease oceanic and soil N<sub>2</sub>O emissions, respectively (McPhadden *et al.*, 1998;  
125 Ishijima *et al.*, 2009; Babbin *et al.*, 2015).

Studies of the stratospheric influence on surface N<sub>2</sub>O variability have differed with respect to the  
relative impact on the NH and SH. Ray *et al.* (2020) found direct correlations between the stratospheric  
Quasi-Biennial Oscillation (QBO), lagged 8-12 months, and the observed surface N<sub>2</sub>O AGR, but in the  
30 SH only. The QBO is a tropical, stratospheric, downward-propagating zonal wind variation, with an  
average period of ~28 months, that dominates the variability of tropical lower stratospheric meteorology  
(Baldwin *et al.*, 2001; Butchart, 2014). Ruiz *et al.* (2021) found a direct correlation between the QBO  
and N<sub>2</sub>O photochemical loss rates in the tropical middle stratosphere, but concluded that interannual  
variability in surface N<sub>2</sub>O globally was governed more by QBO-related changes in the dynamical  
135 processes of the lowermost stratosphere. They showed evidence for a coherent influence of cross-  
[tropopause transport](#) on the surface N<sub>2</sub>O seasonal cycle in the NH but not the SH.

Deleted: El Niño Southern Oscillation (

Deleted: )

Deleted: northern hemisphere (

Deleted: )

Deleted: southern hemisphere (

Deleted: )

Deleted: that, despite a clear

Deleted: ,

Deleted: appeared to be

Deleted: by cross-tropopause transport and mixing, rather than  
directly by the

Deleted: .

Deleted: those dynamics

Nevison *et al.* (2011) argued that cross-tropopause transport and mixing drives the N<sub>2</sub>O seasonal minimum in both hemispheres, based on significant correlations between surface N<sub>2</sub>O seasonal anomalies and stratospheric indices reflective of the Brewer-Dobson Circulation (BDC). The BDC is a planetary-wave-driven, large-scale meridional circulation that transports ozone, greenhouse gases, and other constituents poleward and maintains the thermal structure of the stratosphere (Butchart, 2014; Minganti *et al.*, 2020). As part of this transport, the BDC brings N<sub>2</sub>O-poor air from the tropical middle and upper stratosphere into the polar lower stratosphere in the winter hemisphere (Liang *et al.*, 2008; 2009; Nevison *et al.*, 2011).

**Deleted:** circulation

**Deleted:** warm,

**Moved (insertion) [1]**

**Deleted:** PLST reflects the cumulative effect of fall/winter stratospheric downwelling due to the BDC (Holton, 2004).

A better grasp of the controls on tropospheric N<sub>2</sub>O variability has important implications for the interpretation of biogeochemical signals in N<sub>2</sub>O data. If abiotic factors associated with the downward transport of N<sub>2</sub>O-poor air from the stratosphere contribute significantly to variability, they must be disentangled from the data before inferring information about surface biogeochemistry and emissions. Understanding the influence of stratospheric variability on surface N<sub>2</sub>O also may provide insight into anomalous changes in the AGR of CFC-11, which has a stratospheric sink similar to that of N<sub>2</sub>O (Ray *et al.*, 2020; Ruiz *et al.*, 2021; Lickley *et al.*, 2021).

This paper explores the causes of variability in both the seasonal cycle and the AGR of tropospheric N<sub>2</sub>O. It follows up on previous work by Nevison *et al.* (2011), who inferred a stratospheric influence in surface atmospheric N<sub>2</sub>O data based entirely on correlations between interannual variations in stratospheric indices and detrended N<sub>2</sub>O anomalies in months surrounding the seasonal N<sub>2</sub>O minimum. In the meantime, observed altitude-latitude cross sections have become available from aircraft surveys that span a full seasonal cycle. In addition, advances in model development allow for explicit simulation of stratospheric N<sub>2</sub>O tracers (Ruiz *et al.*, 2021; Liang *et al.*, 2022).

This study uses the NASA Goddard GEOS-5 Chemistry-Climate Model (GEOSCCM), which includes a tagged stratospheric N<sub>2</sub>O tracer that is transported individually in the model and can be distinguished from tropospheric tracers of fresh surface emissions (Liang *et al.*, 2022). The study also examines

atmospheric N<sub>2</sub>O data collected in the NH by the National Oceanic Atmospheric Administration (NOAA) during routine aircraft monitoring, as well as N<sub>2</sub>O data measured by recent global airborne surveys spanning both hemispheres. Finally, it performs an updated correlation analysis of surface N<sub>2</sub>O anomalies from ground-based NOAA sites against ENSO and QBO indices as well as polar lower stratospheric temperature (PLST), which is used as a tracer for the BDC, with the assumption that significant correlations provide support (although not proof) for causation.

Formatted: Subscript

Deleted: and collected by the National Oceanic Atmospheric Administration (NOAA) during routine aircraft monitoring in the NH...

Deleted: reflects the influence of

190 The paper is organized as follows: Section 2 describes the data and methods used. Section 3 presents the results, beginning in Section 3.1 with an examination of climatological mean seasonal cycles and latitude-altitude cross sections of N<sub>2</sub>O from GEOSCCM and aircraft data. Section 3.2 examines correlations between variability in the N<sub>2</sub>O AGR from NOAA long-term surface monitoring data, PLST, and indices of QBO and ENSO. Section 3.3 examines correlations between PLST and variability in monthly N<sub>2</sub>O anomalies near the month of seasonal minimum. Sections 3.2 and 3.3 include parallel correlation analyses of variability in GEOSCCM N<sub>2</sub>O sampled at NOAA surface sites and GEOSCCM-based QBO and PLST indices. Section 4 interprets and discusses the results. Section 5 finishes with a summary and future outlook.

Deleted: , with the premise that significant correlations offer evidence of causation

Deleted: variability

Deleted: conclusion

## 2. Methods

### 200 2.1 GEOSCCM with tagged stratospheric tracers

GEOSCCM was used to simulate atmospheric N<sub>2</sub>O with geographically resolved surface emissions from soil, ocean and anthropogenic sources, and full stratospheric chemistry with stratospheric N<sub>2</sub>O destruction due to photolysis and O(<sup>1</sup>D) oxidation (Nielsen *et al.*, 2017; Liang *et al.*, 2022). GEOSCCM has been evaluated extensively in multi-model assessments and shown to represent well the mean atmospheric circulation, the interhemispheric exchange rate, the mean age of air in the tropical and polar stratosphere, and the mean atmospheric lifetime of N<sub>2</sub>O (Liang *et al.*, 2022 and references therein). For the current study, GEOSCCM was run at 1°x1° resolution with 72 vertical layers from the surface to 0.01 hPa. In addition to the standard total N<sub>2</sub>O tracer, four additional N<sub>2</sub>O tracers were included to track: 1) aged air from the stratosphere (N<sub>2</sub>O<sub>ST</sub>), and 2) soil, 3) ocean, and 4) anthropogenic

sources freshly emitted in the troposphere. Following the approach of *Liang et al. (2008)*, the tropospheric tracers become the stratospheric tracer,  $N_2O_{ST}$ , when they are transported across the tropopause, and retain that identity even when  $N_2O_{ST}$  re-enters the troposphere, thereby providing a model estimate of the stratospheric influence on tropospheric  $N_2O$ .

The full GEOSCCM simulation spanned 1980-2019, but this study focuses on the final 20 years from 2000-2019 for the correlation analysis between model surface  $N_2O$  anomalies and QBO and PLST. As described in detail in *Liang et al. (2022)*, the GEOSCCM  $N_2O$  lifetime decreased slightly after 2000 (from  $119 \pm 2$  yr in the 1990s down to  $116 \pm 2$  yr in the 2010s) and model emissions were optimized to account for the observed change in the atmospheric  $N_2O$  growth rate. GEOSCCM temperature and QBO do not necessarily correspond to observations since both are internally generated by the GEOS general circulation model, which is free running rather than forced by a reanalysis meteorology.

GEOSCCM QBO and PLST were computed in the same way as the observed indices, as described below in Section 2.4.1 and 2.4.2, respectively. The GEOSCCM  $N_2O$  fields were saved as monthly means and were detrended and converted to anomalies by subtracting a deseasonalized fit to the model time series sampled at Mauna Loa (MLO). The  $N_2O$  time series at MLO is a good proxy for the global  $N_2O$  trend and thus its subtraction provides a convenient, single-station approach for calculating anomalies of the  $N_2O$  mixing ratio for contour plots.

## 2.2 $N_2O$ Data

### 2.2.1 Surface $N_2O$ from NOAA long-term monitoring sites

Surface atmospheric  $N_2O$  data were obtained from the NOAA Global Monitoring Laboratory (GML) for comparison to GEOSCCM output. NOAA has two programs that measure  $N_2O$ , Halocarbons and other Atmospheric Trace Species (HATS, *Thompson et al., 2004*) and the Carbon Cycle Greenhouse Gases group (CCGG, *Lan et al., 2022*). HATS provides *in situ* data measured every ~ 60 minutes using the Chromatograph for Atmospheric Trace Species (CATS) instruments at 5 baseline sites (Barrow, Alaska; Niwot Ridge, Colorado; Mauna Loa, Hawaii; Cape Grim, Tasmania; and South Pole, Antarctica). CCGG maintains a flask-air sampling network at ~55 widely distributed surface sampling

**Deleted:** down from  $119 \pm 2$  yr in the 1990s

**Deleted:** However,

**Deleted:** they

**Deleted:** QBO and PLST

**Formatted:** Font: 12 pt, Not Bold

**Formatted:** Font: Not Bold

**Formatted:** Font: Not Bold, Subscript

**Formatted:** Font: Not Bold

**Formatted:** Font: 12 pt, Not Bold

**Formatted:** Font: 12 pt, Not Bold

**Formatted:** Font: Times New Roman, 12 pt, Not Bold

**Formatted:** Font: Times New Roman, 12 pt, Not Bold, Subscript

**Formatted:** Font: Times New Roman, 12 pt, Not Bold

**Formatted:** Font: Not Bold

**Formatted:** Font: 12 pt, Not Bold

**Formatted:** Subscript

**Formatted:** Font: (Default) Times New Roman

**Deleted:** ) (

**Deleted:** ) (

250 sites, in which duplicate samples are collected about weekly and shipped to Boulder, Colorado for analysis by gas chromatography (GC) with electron capture detection and by a Tunable Infrared Laser Direct Absorption Spectroscopy (TILDAS) after August, 2019. The instruments are calibrated with a suite of standards on the WMO X2006A scale maintained by NOAA GML (Hall et al., 2007). Uncertainties of the measurements (68% confidence interval) range from 0.26 to 0.43 ppb with GC-  
255 ECD and 0.16 ppb with TILDAS. The mean uncertainties in CATS GC data are 0.2 to 1.2 ppb (68% confidence interval) over most of the 2000s, with an increase in recent years as the instruments age.

Deleted: approach their lifetime

This study used the NOAA combined HATS/CCGG N<sub>2</sub>O product from 1998-2021, which is based on monthly medians from the CATS *in situ* program (at the 5 HATS baseline sites) and monthly means  
260 from the CCGG flask program at a selected subset of 12 of the ~55 total sites, (https://doi.org/10.15138/GMZ7-2Q16; Hall et al., 2007). All of the NOAA sites considered in this study are long-standing remote sites situated away from strong local anthropogenic sources. They include Alert, Canada; Summit, Greenland; Mace Head, Ireland; Trinidad Head, California, Cape Kumakahi, Hawaii, Cape Matatula, Samoa; Palmer Station, Antarctica and the 5 HATS baseline sites  
265 (at which CCGG also makes overlapping flask measurements). In addition to these 12 individual sites, global, NH and SH means are estimated from the latitude-binned and mass-weighted means of the combined monthly means for the 12 sites (Hall et al., 2011). The combined monthly data are first aggregated at the measurement program level for each sampling location. At sites where both HATS and CCGG measure, a weighted mean is calculated based on the programs' monthly uncertainties.

Deleted: 0

Deleted: (

Deleted: 3

Deleted: background

Deleted: )

Deleted: If both

Deleted: at a location

Deleted: All of the NOAA sites considered in this study, including Alert, Canada; Summit, Greenland; Mace Head, Ireland; Cape Matatula, Samoa; Palmer Station, Antarctica and the HATS baseline sites listed above, are long-standing remote sites situated away from strong local anthropogenic sources. In addition to these individual sites, global, NH and SH means are estimated from the latitude-binned and mass-weighted means of the combined monthly means for 12 background sites (Hall et al., 2011).

Deleted: E

Deleted: B

### 270 2.2.2 NOAA empirical background for atmospheric N<sub>2</sub>O

The NOAA empirical background is a 4-dimensional (4-D) field, constructed from NOAA surface and aircraft N<sub>2</sub>O data, which is used in North American regional inversions to represent the background concentration of atmospheric N<sub>2</sub>O prior to the influence of continental surface fluxes (Nevison et al., 2018). The 4-D field is defined daily over North America from 500-7500 m every 1000 m, from 170°-  
275 50°W every 10° longitude, and from 20-70°N every 5° latitude (or, prior to 2017, from 20-80°N every 10° latitude). For this study, a deseasonalized fit to the NOAA time series at Mauna Loa was used to

Deleted: To construct the field, NOAA data are categorized as marine boundary layer, free troposphere or continental boundary layer, depending on the location of each sample. These three categories are treated individually as follows: For the marine boundary layer, time- and latitude-dependent reference surfaces are computed separately for the Pacific and Atlantic (Masarie and Tans, 1995, updated as described in Lan et al., 2023). For the free-troposphere, reference surfaces are created using a similar approach, with an additional "domain-filling" step informed by backward and forward trajectories for each aircraft sample collected above 3000 m AGL. For the continental boundary layer, N<sub>2</sub>O data are detrended by subtracting the latitude and time dependent marine boundary layer reference values, where the transition from Pacific to Atlantic is represented by linear interpolation as a function of longitude across the continent. Then, a multi-year mean seasonal cycle is computed as a function of latitude, longitude, and day of year following Hammerling et al. (2012).

detrend and remove the mean value (centered in the mid troposphere) of the empirical background data, thus allowing them to be collapsed into a single climatological year and presented as anomalies. The climatology encompassed January 1, 2005–December 31, 2013, a period when atmospheric N<sub>2</sub>O was  
315 increasing by about 0.9 ppb/yr.

### 2.2.3 N<sub>2</sub>O data from global airborne surveys

Atmospheric N<sub>2</sub>O measurements were made *in situ* with the Harvard/Aerodyne Quantum Cascade Laser Spectrometer (QCLS) on three different aircraft campaigns designed to study the atmospheric profiles of greenhouse and related gases (*Wofsy et al., 2011; Stephens et al., 2018*). QCLS N<sub>2</sub>O data  
320 are retrieved at 1-Hz with 1s precision of 0.09 ppb and reproducibility with respect to the WMO N<sub>2</sub>O scale of 0.2 ppb (*Kort et al., 2011; Santoni et al., 2014*) on the NOAA-2006 scale (*Hall et al., 2007*).

The first of the campaigns, the **High-performance Instrumented Airborne Platform for Environmental Research (HIAPER)** Pole to Pole Observations (HIPPO) project, consisted of 5 roughly month-long sets  
of flights centered over the central Pacific Ocean extending from the surface to the upper

325 troposphere/lower stratosphere and nearly pole to pole (*Wofsy et al., 2011*). The flights were timed between January 2009 and November 2011 to create a climatological seasonal cycle. The second

campaign, **O<sub>2</sub>/N<sub>2</sub> Ratio and CO<sub>2</sub> Airborne Southern Ocean (ORCAS)**, took place in January-February 2016 and focused on the Southern Ocean south of ~35°S (*Stephens et al., 2018*). Most recently,  
330 the Atmospheric Tomography Mission (ATom) campaign extended nearly pole to pole over both the Pacific and Atlantic Oceans. ATom consisted of 4 deployments over 3 years, with each deployment approximately 1 month long (*Thompson et al., 2022*). QCLS N<sub>2</sub>O was measured during the second

through fourth ATom deployments in January/February 2017, September/October, 2017 and April/May 2018, respectively, but N<sub>2</sub>O measurements are not available from the first ATom deployment in  
335 July/August 2016 due to technical problems (*Gonzalez et al., 2021*). For all figures presented below using QCLS N<sub>2</sub>O, the flight track data were interpolated onto a 5 degree latitude by 50 hPa grid using the akima package in R (Akima, 1978). In addition, a deseasonalized fit to the NOAA time series at Mauna Loa was subtracted from all data, allowing them to be collapsed into a climatological year and expressed as anomalies.

**Deleted:** time period selected for the

**Deleted:** w

**Deleted:** as

**Deleted:** 9

**Deleted:** which roughly overlaps with the HIPPO airborne surveys described below, over

**Deleted:** the

**Deleted:** se

**Formatted:** Font: (Default) +Body (Times New Roman), 12 pt

**Deleted:** HIAPER

**Deleted:** se

**Deleted:**

**Formatted:** Font: (Default) +Headings (Times New Roman), 12 pt

**Formatted:** Font: (Default) +Headings (Times New Roman), 12 pt, Subscript

**Formatted:** Font: (Default) +Headings (Times New Roman), 12 pt

**Formatted:** Font: (Default) +Headings (Times New Roman), 12 pt, Subscript

**Formatted:** Font: (Default) +Headings (Times New Roman), 12 pt

**Formatted:** Font: (Default) +Headings (Times New Roman), 12 pt, Subscript

**Formatted:** Font: (Default) +Headings (Times New Roman), 12 pt

**Formatted:** Font: (Default) +Headings (Times New Roman)



350 **2.3 Mean seasonal cycles and interannual variability in surface N<sub>2</sub>O**

Mean seasonal cycles for NOAA surface N<sub>2</sub>O observations and GEOSCCM N<sub>2</sub>O tracers were estimated using a bootstrapping method in which 20% of the timeseries was randomly removed and the remaining 80% was fit to a 3<sup>rd</sup> order polynomial plus first 4 harmonics. These steps were repeated over 500 iterations to estimate the range of uncertainty in the harmonic components of the fit.

**Deleted:** Correlation analysis for

**Formatted:** Font: Bold, Font color: Auto

**Formatted:** Space Before: 12 pt, After: 12 pt, Line spacing: single, Widow/Orphan control, Tab stops: Not at 0.39" + 0.78" + 1.17" + 1.56" + 1.94" + 2.33" + 2.72" + 3.11" + 3.5" + 3.89" + 4.28" + 4.67"

355 **Interannual variability in the atmospheric growth rate of N<sub>2</sub>O in the NOAA surface NH, SH and global time series** was calculated by first removing the seasonal cycle from the monthly mean time series by computing a 12-month running average,

**Formatted:** Font color: Black

**Formatted:** Space Before: 0 pt, After: 3 pt, Line spacing: 1.5 lines, No widow/orphan control, Tab stops: 0.39", Left + 0.78", Left + 1.17", Left + 1.56", Left + 1.94", Left + 2.33", Left + 2.72", Left + 3.11", Left + 3.5", Left + 3.89", Left + 4.28", Left + 4.67", Left

**Deleted:** 2.3.1 Interannual variability in the atmospheric growth rate

$$X_i = (C_{i-6} + 2 \sum_{k=i-5}^{i+5} C_k + C_{i+6})/24, \quad (1)$$

360 where  $C$  is the original monthly mean time series and  $X$  is the deseasonalized time series. The slope of the deseasonalized time series then was computed as a central difference,

$$S_i = 12 \frac{X_{i+1} - X_{i-1}}{2}, \quad (2)$$

365 where  $S$  is the centrally differenced slope and the scalar 12 converts  $S$  from units of ppb/month to ppb/yr. To account for the increasing growth rate of atmospheric N<sub>2</sub>O, the absolute slopes  $S$  were converted to atmospheric growth rate anomalies by removing an optimal (increasing) linear fit determined by recursive least squares regression.

**Deleted:** 2.3.2 Interannual variability in the magnitude of the seasonal N<sub>2</sub>O minimum

370 **Interannual anomalies in the magnitude of the seasonal minimum** were calculated by detrending the raw monthly mean N<sub>2</sub>O data with a 3<sup>rd</sup>-order polynomial, after which a climatological seasonal cycle was constructed by taking the average of the detrended data for all Januaries, Februaries, etc. This climatological annual cycle was subtracted from the original raw data to produce a deseasonalized (but not detrended) time series. A running 12-month annual mean of this curve was then computed as in Equation 1, but where  $C$  is now the deseasonalized time series rather than the original monthly mean

**Deleted:** To calculate  $i$

**Deleted:** ,

**Deleted:** were detrended

time series. This analysis focused on mid and high latitude sites in the NOAA dataset. At stations with  
385 gaps in the monthly data, the original 3<sup>rd</sup> order polynomial fit was used as a placeholder in the running  
mean. The running mean was subtracted from the deseasonalized curve to remove the secular trend and  
other low frequency variability, thus isolating the residual high frequency anomalies.

## 2.4 Proxies and indices for the correlation analysis

The computation of N<sub>2</sub>O AGR anomalies from Section 2.3, created a set of monthly-resolved time series  
390 for the SH, NH and global means. These were plotted against various proxies and indices for  
stratospheric influences and ENSO. In addition, the high frequency residuals from Section 2.3, at  
various mid and high latitude sites were sorted by month and selected months were plotted against  
PLST as described below in Section 2.4.1. The PLST proxy involves a single value for each year, such  
that correlation coefficients and p values were computed based on the number of years N with data. For  
395 the ENSO and QBO indices, the correlation statistics were computed based on the reduced, effective N  
(N<sub>eff</sub>) number of monthly data points after accounting for the autocorrelation that is introduced by the  
12-month running mean used to compute the N<sub>2</sub>O AGR (see Supplementary text S1 for more details.)

### 2.4.1 Polar lower stratospheric temperature (PLST) as proxy for the Brewer Dobson Circulation

Mean polar (60°-90°) lower stratospheric temperature at 100 hPa in January-March (winter) in the NH  
400 and September-November (spring) in the SH was computed from the Modern-Era Retrospective  
Analysis for Research Applications, Version 2 (MERRA-2) reanalyses (Gelaro *et al.*, 2017). The mean  
PLST in each hemisphere was treated as a proxy for the integrated strength of the BDC, which brings  
N<sub>2</sub>O-poor air from the middle to upper tropical stratosphere into the polar winter lower stratosphere  
through diabatic descent. PLST represents the cumulative effect of descent throughout fall and winter,  
405 with warmer PLST corresponding to stronger descent (Holton, 2004; Nevison *et al.*, 2007; 2011).  
Winter months (January-March) were averaged in the NH and spring months (September-November) in  
the SH to account for the later seasonal breakup of the Antarctic polar vortex compared to the Arctic  
polar vortex (Nevison *et al.*, 2011). For the monthly analysis, the PLST proxy was regressed against the  
monthly N<sub>2</sub>O anomaly in each of the subsequent months leading up to and encompassing the seasonal

Deleted: ¶

Deleted: .1

Deleted: proxies and

Deleted: r both

Deleted: .2

Deleted: the polar lower stratospheric temperature (PLST) BDC

Deleted: proxy

Deleted:

Formatted: Subscript

Deleted: circulation

Moved up [1]: PLST reflects the cumulative effect of fall/winter stratospheric downwelling due to the BDC (Holton, 2004).

Deleted: warm

Deleted: downwelling

Formatted: Font: Italic

minimum in tropospheric N<sub>2</sub>O, which occurs in summer in the NH and autumn in the SH. For the AGR analysis, the mean N<sub>2</sub>O AGR anomaly was averaged over 12 months (considering a range of start/end months) for regression against PLST.

#### 2.4.2 Quasi-Biennial Oscillation (QBO)

The QBO was quantified using monthly mean stratospheric zonal wind values in m/s derived from twice daily balloon radiosondes conducted by the Meteorological Service Singapore Upper Air Observatory at a station located at 1.34°N, 103.89°E ([https://acd-ext.gsfc.nasa.gov/Data\\_services/met/qbo/QBO\\_Singapore\\_Uvals\\_GSFC.txt](https://acd-ext.gsfc.nasa.gov/Data_services/met/qbo/QBO_Singapore_Uvals_GSFC.txt)). A positive QBO indicates westerly winds and a negative QBO indicates easterly winds. A range of altitudes from 10 mb to 100 mb was considered. Since the QBO index is a monthly mean time series, it can be compared directly to the monthly mean N<sub>2</sub>O AGR time series. However, delays are expected between the QBO and its influence on tropospheric N<sub>2</sub>O (*Strahan et al.*, 2015; *Ray et al.*, 2020). Therefore, a range of lag times was considered spanning 6-24 months when correlating with the N<sub>2</sub>O AGR anomalies to identify the optimal QBO altitude and lag in each hemisphere.

#### 2.4.3 ENSO

ENSO cycles were defined using the Niño 3.4 index, which is based on sea surface temperature anomalies from 5°S to 5°N and 170° to 120°W. The Niño 3.4 index defines an El Niño event as a temperature anomaly of > 0.4 °C, and a La Niña event as a temperature anomaly of < -0.4 °C. Monthly Niño 3.4 indices were obtained from <https://www.cpc.ncep.noaa.gov/data/indices/sstoi.indices>. Like the QBO index, Niño 3.4 is a monthly time series that can be compared directly to the monthly mean N<sub>2</sub>O AGR time series. In the analysis presented here, a range of lag times in the Niño 3.4 index was considered spanning 0-12 months to identify the optimal lag in each hemisphere.

Deleted: degrees C

#### 2.5 GEOSCCM correlation analysis

Equations 1 and 2 were applied to GEOSCCM N<sub>2</sub>O output sampled at the coordinates of NOAA monitoring sites to create modeled N<sub>2</sub>O AGR time series and monthly anomalies, using both total N<sub>2</sub>O and N<sub>2</sub>O<sub>ST</sub>. Similarly, mean winter and spring PLST at 100 hPa was calculated for GEOSCCSM

450 output in the NH and SH, respectively, as described in Section 2.4.1, for each model year from 2000-  
2019. Finally, a GEOSCCM monthly QBO index was calculated at a range of altitudes from 10 mb to  
100 mb by averaging the model zonal wind component in m/s between 5°S and 5°N over each of the  
240 months from 2000-2019. A correlation analysis was performed using the GEOSCCM N<sub>2</sub>O AGR  
and monthly anomaly time series regressed against GEOSCCM PLST and QBO, similar to that  
455 described for the observed quantities in Sections 2.3-2.4. The ENSO correlation analysis was not  
applied to GEOSCCM output because the model did not attempt to reproduce the impact of ENSO on  
surface flux variability (*Liang et al., 2022*).

### 3. Results

#### 3.1 Stratospheric influence on tropospheric N<sub>2</sub>O in model and aircraft data

460 Figure 1 shows that the GEOSCCM N<sub>2</sub>O mean seasonal cycle at surface sites is dominated by  
stratospheric air depleted in N<sub>2</sub>O that is transported to the surface, rather than by the influence of  
surface sources. However, the surface emissions tend to pull the total N<sub>2</sub>O seasonal minimum about 1  
month earlier than the N<sub>2</sub>O<sub>ST</sub> minimum at most sites. Figure 1 also shows that GEOSCCM captures the  
mean observed seasonal cycle in N<sub>2</sub>O relatively well at sites in the SH but overestimates the amplitude  
465 of the cycle at sites in the NH, with a ~1-2 month delay in phasing relative to observations.

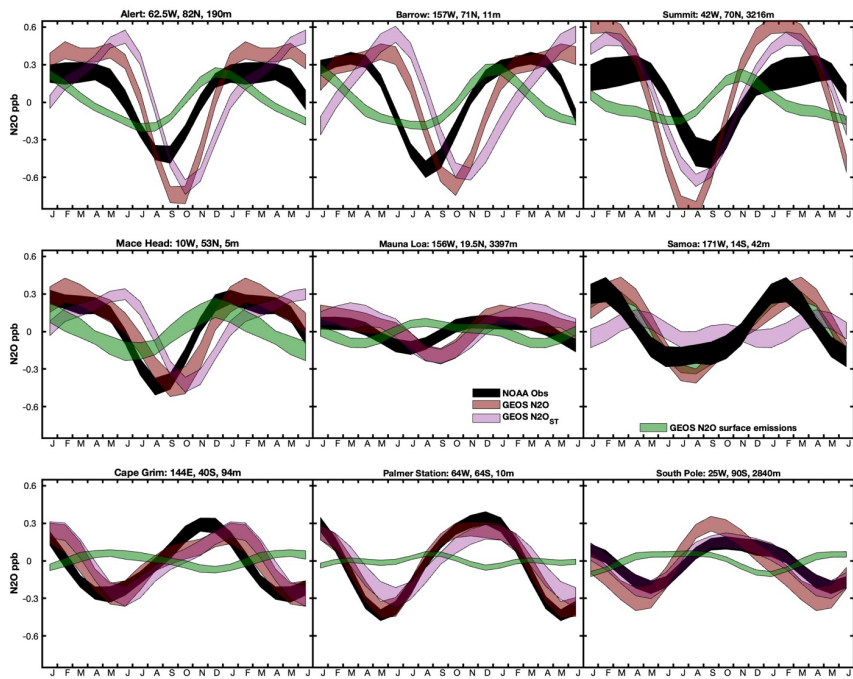
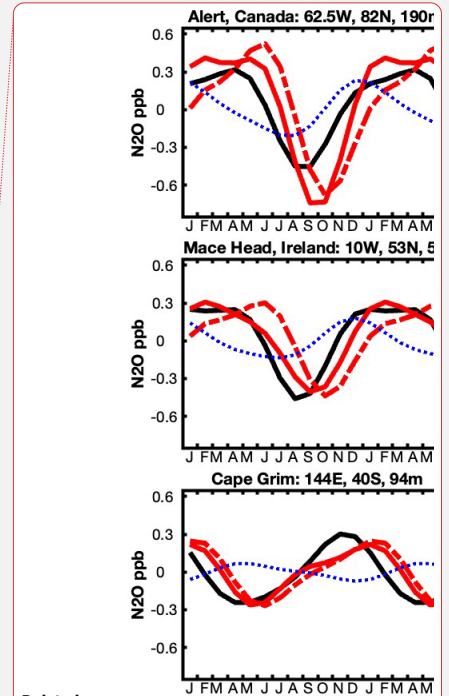


Figure 1: Detrended seasonal cycles in  $N_2O$  mixing ratio (ppb) modeled by GEOSCCM and compared to NOAA surface station data at 9 surface sites. Top row from left to right: Alert (Canada), Barrow (Alaska), Summit (Greenland); middle row from left to right: Mace Head (Ireland), Mauna Loa (Hawaii), Cape Matatula (Samoa); bottom row from left to right: Cape Grim (Tasmania), Palmer Station (Antarctica), South Pole (Antarctica). **Black** is observed  $N_2O$  from NOAA. For GEOSCCM, the total  $N_2O$  from all forcings is in red and the stratospheric tracer  $N_2O_{ST}$  is in **magenta**. **Blue** is  $N_2O$  due to fresh surface emissions, representing the combined net influence of the natural soil, ocean, and anthropogenic atmospheric tracers.



Deleted:

Deleted: atmospheric

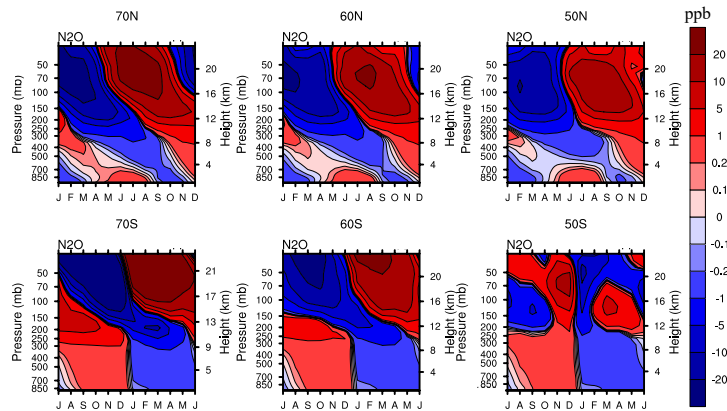
Deleted: The black heavy line

Deleted: dashed red

Deleted: The dotted blue line

470  
475 Figure 2 provides a two-dimensional view, using zonally-averaged altitude-month contour plots at middle and high latitudes in both hemispheres, of how the signal of stratospheric air depleted in  $N_2O$  is transmitted to the surface in GEOSCCM. This  $N_2O$ -poor air accumulates during winter (starting in ~December in the NH and ~July in the SH) in the polar stratosphere, descends vertically and crosses into the troposphere in spring (March-April) in the NH and early summer (January-February) in the SH.

485 The SH latitude panels in Fig. 2 are plotted with a 6-month shift to help visualize the later seasonal phasing of the stratospheric influence in the SH relative to the NH. After crossing into the troposphere, the N<sub>2</sub>O-poor air continues to move downward, and also mixes equatorward, from approximately January to May at SH mid-to-high latitudes and April to October at NH mid-to-high latitudes (Liang et al., 2009; 2022). Due to lags in downward propagation and mixing, the modeled surface minimum in the lower troposphere does not occur until late summer to early autumn in both hemispheres (Fig. 1 and 2). Supplementary Figure S1 shows a 3-dimensional view of this process in a series of 12 monthly altitude by latitude plots.



495 **Figure 2:** GEOSCCM anomalies of N<sub>2</sub>O mixing ratio (ppb) as a function of month and altitude over a mean seasonal cycle, plotted from the surface to 30 hPa in the NH (top row) and SH (bottom row). From left to right: 10° latitude bins centered at 70°, 60° and 50°. Monthly anomalies are computed by subtracting the annual mean value at each pressure level.

Figure 3 shows that the NOAA N<sub>2</sub>O empirical background, when organized as a series of zonally-averaged altitude-month contour plots at NH latitudes, has features similar to those simulated by GEOSCCM. Both model and observations show a signal of N<sub>2</sub>O depletion beginning in early spring in the upper troposphere that propagates down to the surface. In both model and observations, the signal is strongest at high latitudes and weakens substantially moving equatorward. However, the NOAA data suggest a faster, more direct downward propagation of the stratospheric signal, which arrives at the

**Deleted:** Figure

**Formatted:** Font: Italic

**Deleted:** Figure

**Deleted:** s

**Deleted:** N<sub>2</sub>O anomalies in ppb

**Formatted:** Normal (Web), Space Before: 0.1 pt, After: 0.1 pt, Line spacing: 1.5 lines, Widow/Orphan control, Tab stops: Not at 0.39" + 0.78" + 1.17" + 1.56" + 1.94" + 2.33" + 2.72" + 3.11" + 3.5" + 3.89" + 4.28" + 4.67"

surface in August-September, compared to September-October in GEOSCCM. As a result, the phasing of the GEOSCCM surface minimum is delayed ~1-2 months relative to the NOAA empirical background, consistent with the comparison to NOAA surface monitoring data in Fig. 1.

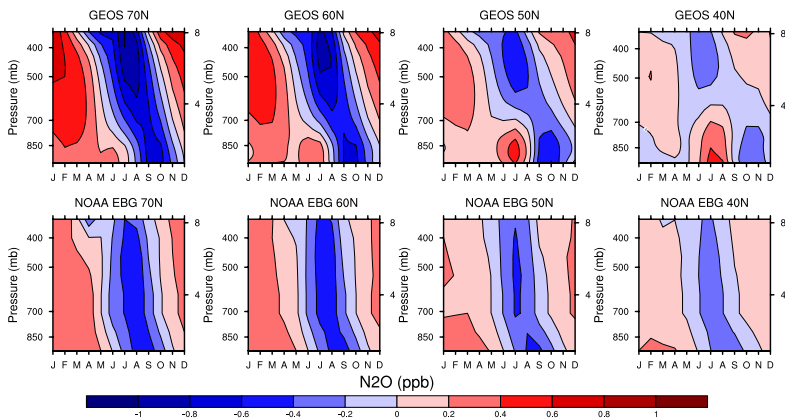


Figure 3: Anomalies of N<sub>2</sub>O mixing ratio (ppb) as a function of month and altitude over a mean seasonal cycle, plotted from the surface to 8 km (~330 hPa) in the NH for GEOSCCM (top row) and the NOAA empirical background (bottom row). From left to right: 10° latitude bins centered at 70°, 60°, 50° and 40°N. Monthly anomalies are computed by subtracting the annual mean value at each pressure level.

The positive anomalies in Fig. 3 also differ between model and observations, with surface features centered on July at 40°-50°N in GEOSCCM, which used a summer-dominant soil source (Liang et al., 2022), while the NOAA empirical background shows positive surface anomalies in late winter and spring, likely reflecting North American agricultural sources (Nevison et al., 2018). At 60° and 70°N, the stronger contrast between positive and negative anomalies throughout the atmospheric column in GEOSCCM compared to NOAA reflects the model's larger seasonal cycle, as seen also in Fig. 1.

Figure 4 provides a further perspective on the signal of N<sub>2</sub>O-poor stratospheric air in the NOAA empirical background. When viewed as a 12-month sequence of altitude-latitude contours in the NH, the signal originates at northern polar latitudes in the upper troposphere in late winter and early spring, descends and mixes equatorward, with a peak surface influence around July-September at middle to

Deleted: Figure

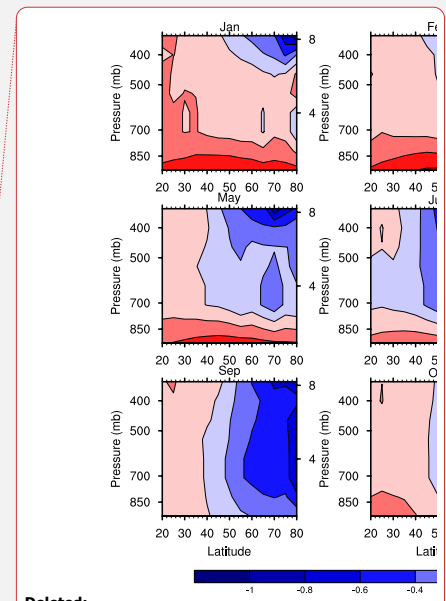
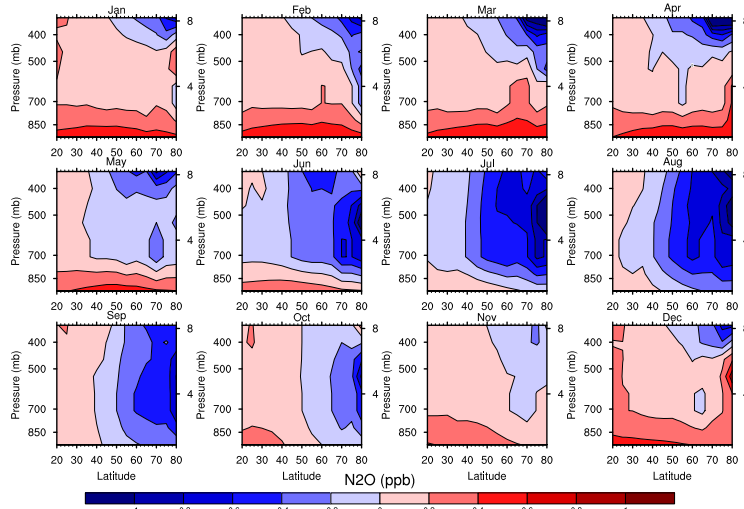
Deleted: ¶

Deleted: N<sub>2</sub>O anomalies in ppb

Formatted: Font: Italic

Deleted: August

high latitudes in the NH that overshadows any surface source signal. By late fall and winter, the signal has dissipated at the surface but is forming again in the upper troposphere.



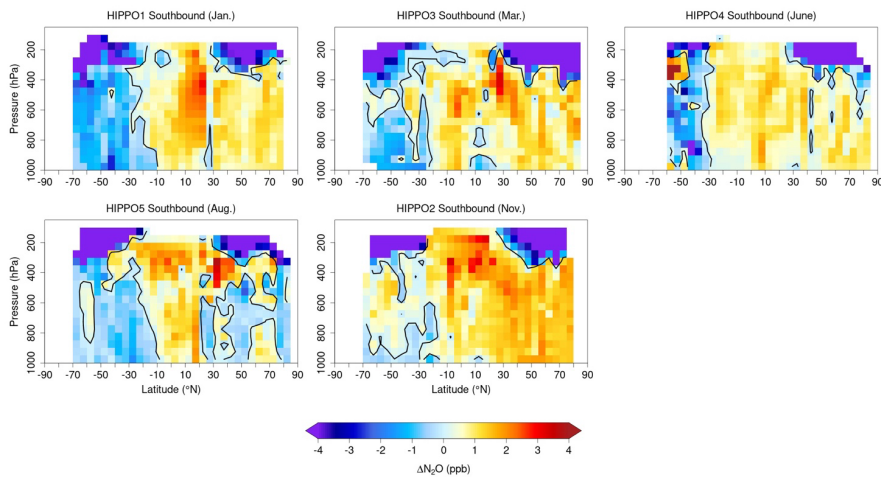
- Deleted:
- Deleted: N<sub>2</sub>O
- Deleted: a
- Deleted: Northern Hemisphere
- Formatted: Subscript
- Deleted: Figure
- Deleted: Figure

Figure 4: Anomalies of N<sub>2</sub>O mixing ratio (ppb) in the NH from the NOAA empirical background, plotted in a monthly sequence of altitude vs. latitude plots extending from the surface up to 8 km (~330 hPa) and from 20°N-80°N.

QCLS N<sub>2</sub>O data from airborne surveys extend up to 14 km and thus provide a broader perspective with respect to altitude of the stratospheric influence on tropospheric N<sub>2</sub>O. Of the 3 airborne surveys available for our analysis (HIPPO, ORCAS and ATom), HIPPO provides the most complete N<sub>2</sub>O time series across all seasons. In Fig. 5, the southbound transects from the five HIPPO deployments are detrended and arranged chronologically as altitude-latitude contour plots over an annual mean cycle. These plots form a sequence with a similar movement of N<sub>2</sub>O-poor stratospheric air from upper levels down to the surface as seen in GEOSCCM and the NOAA empirical boundary data. This progression is most readily seen in the NH in Fig. 5, in which N<sub>2</sub>O-poor air in the polar lower stratosphere has crossed the tropopause by March. By June it has descended into the middle troposphere and started moving



555 equatorward, reaching its maximum influence at the surface in August. By October/November, the stratospheric signal is no longer visible at the surface following tropospheric mixing and dilution. This seasonal progression is also evident in a fuller dataset that also includes the ATom and northbound HIPPO transects collapsed into a climatological cycle (Supplementary Fig. S2)



560 **Figure 5:** Sequence of five HIPPO pressure-latitude contours of anomalies of  $N_2O$  mixing ratio (ppb) arranged to form an annual sequence; from left to right: January, March, June (top row) and August, November (bottom row). Each panel represents a north-to-south transect across latitude with vertical profiling from the surface to 14 km.

Deleted: Figure

Deleted: plots

Formatted: Font: 10 pt

Formatted: Subscript

Deleted: an annual sequence

### 3.2 Correlation analysis of the Surface $N_2O$ Atmospheric Growth Rate (AGR)

565 In this section NOAA surface  $N_2O$  AGR anomalies from 1998-2020 are plotted against polar lower stratospheric temperature (PLST) and QBO and ENSO indices, with varying lag times as described in the Methods (Section 2). The analysis focuses on the NOAA global, NH, and SH mean products, with the assumption that a significant correlation between the interannual variability in the  $N_2O$  AGR and one or more of the indices can be interpreted to support a causal influence on the  $N_2O$  AGR. However, correlation does not prove causation and cannot distinguish possible confounding effects, such as the influence of ENSO on both interhemispheric transport and surface sources. A similar correlation

Deleted: premise

Deleted: of the latter

Deleted: .

analysis is performed for the GEOSCCM N<sub>2</sub>O AGR and the model's internally-generated QBO and PLST fields, with the assumption that similarities between modeled and observed correlations may also support a causal influence.

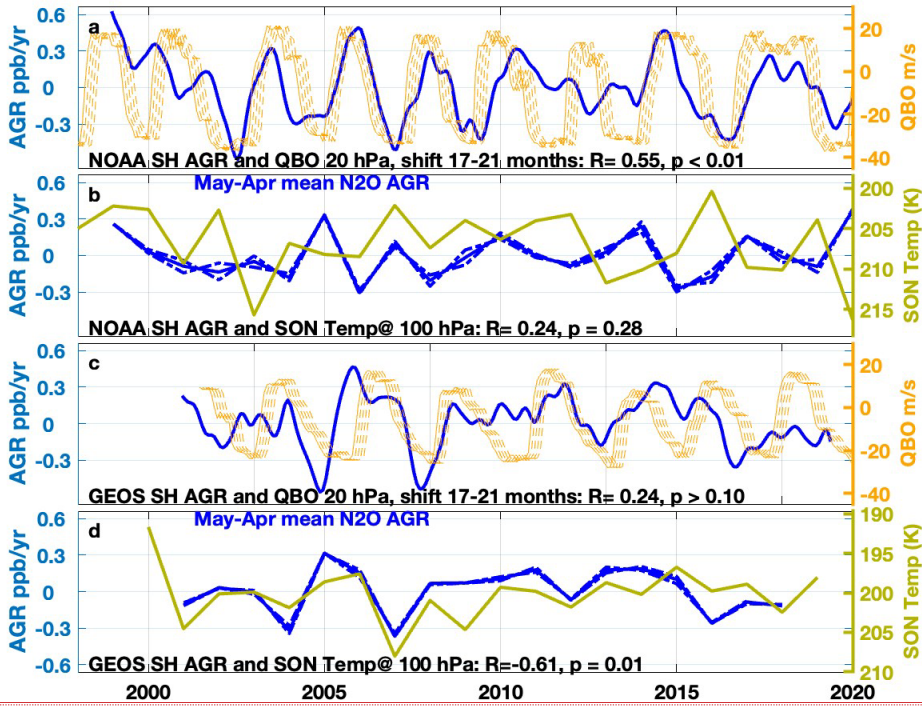
580

Figure 6, which presents correlations between the SH surface N<sub>2</sub>O AGR and the QBO and PLST indices, first for NOAA observations and next for GEOSCCM output, shows that the QBO is positively correlated to the NOAA N<sub>2</sub>O AGR. The optimal correlation ( $R = 0.55$ ,  $p < 0.01$ ) occurs for QBO in the upper stratosphere at 20 hPa with a time shift of about 18 (17-19) months relative to the N<sub>2</sub>O time series. However, spring PLST is not significantly correlated to the NOAA surface N<sub>2</sub>O AGR in the SH (Fig. 6b). The correlation between GEOSCCM QBO and the SH N<sub>2</sub>O AGR is weak ( $R = 0.24$ ,  $p > 0.10$ ) but also positive in sign in the upper stratosphere with an optimal shift in the GEOSCCM QBO of about 19 months, similar to that found for NOAA (Fig. 6c). GEOSCCM PLST is negatively correlated with the N<sub>2</sub>O AGR averaged over a range of different 12-month intervals, with the highest correlation ( $R = -0.61$ ,  $p = 0.01$ ) over the 12-month interval from May-April (Fig. 6d).

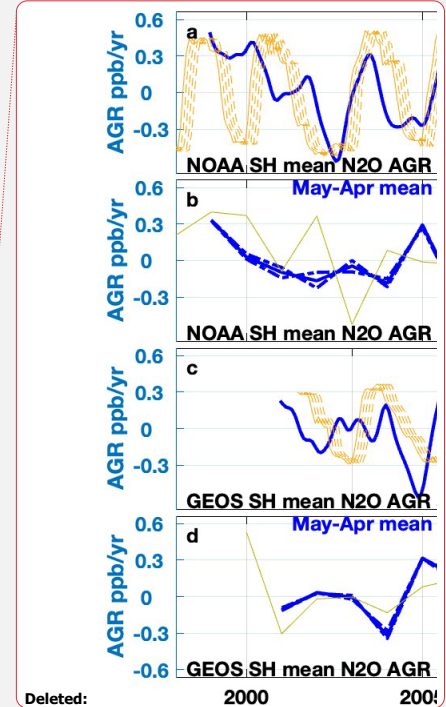
585

590

- Deleted: a
- Deleted: shows
- Formatted: Subscript
- Deleted: in the SH
- Deleted: index
- Deleted: observed surface
- Deleted: , with an
- Deleted: 42
- Deleted: 9
- Deleted: 21
- Deleted: er
- Deleted: simila
- Deleted: r
- Deleted: Figure
- Deleted: ¶  
Spring PLST is not significantly correlated to the NOAA surface N<sub>2</sub>O AGR in the SH (Figure 6b), but within
- Deleted: the two are
- Deleted: (Figure 6d). The correlation with PLST in GEOSCCM occurs for...
- Deleted: strongest
- Deleted: Figure



615 Figure 6: SH N<sub>2</sub>O atmospheric growth rate (AGR in ppb/yr) for (a) NOAA and (c) GEOSCCM plotted with the QBO index at 20 hPa with a 17-21 month forward shift in the index. (b,d) SH N<sub>2</sub>O AGR plotted with mean lower stratospheric temperature averaged over 60-90°S for September-November in the year prior to the annual label on the X axis. The AGR is averaged from monthly N<sub>2</sub>O data over the ensuing 12 month period May-April (solid blue line), shifted plus or minus 1 month (dotted blue lines), for (b) NOAA and (d) GEOSCCM. Note: to convert to %/yr (AGR units often used in the literature) ppb/yr can be multiplied by 100/323 (~1/3), where 323 is the mean tropospheric mixing ratio of N<sub>2</sub>O over 1998-2020.



Deleted:

Deleted: 1

Deleted: t

Deleted: surface

Deleted: in the NH

Deleted: significantly

Deleted: 1

625 Figure 7, which presents the corresponding correlations for the NH surface N<sub>2</sub>O AGR, shows that, in contrast to the SH, the NOAA NH N<sub>2</sub>O AGR is correlated only weakly to the QBO index at all altitudes, and with a negative sign. The highest correlation in the NH occurs for 50 hPa QBO (R= -0.21, p > 0.1) with a 10-14 months lag (Fig. 7a). However the NOAA NH N<sub>2</sub>O AGR is anticorrelated significantly to winter PLST (R = -0.69, p < 0.001), with an optimal correlation for the 12-month period

from July-June encompassing the January-March PLST average (Fig. 7b). GEOSCCM predicts an anticorrelation ( $R = -0.47, p < 0.05$ ) between the QBO and the NH  $N_2O$  AGR, which is optimal around 50 hPa with 10-14 month QBO lag, similar to NOAA (Fig. 7c) and also predicts an anticorrelation between PLST and NH  $N_2O$  AGR (Fig. 7d).

Deleted: Figure

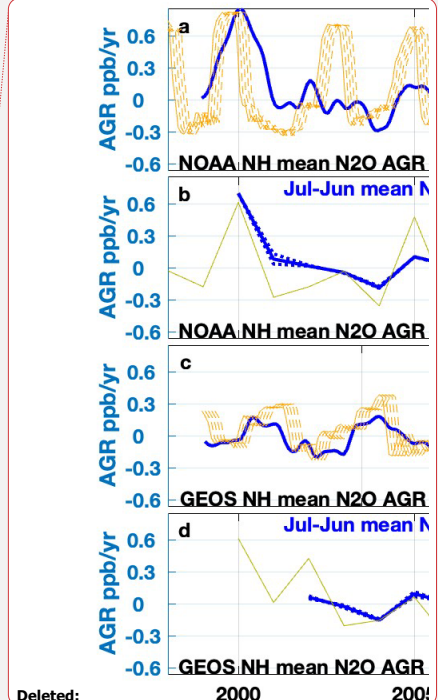
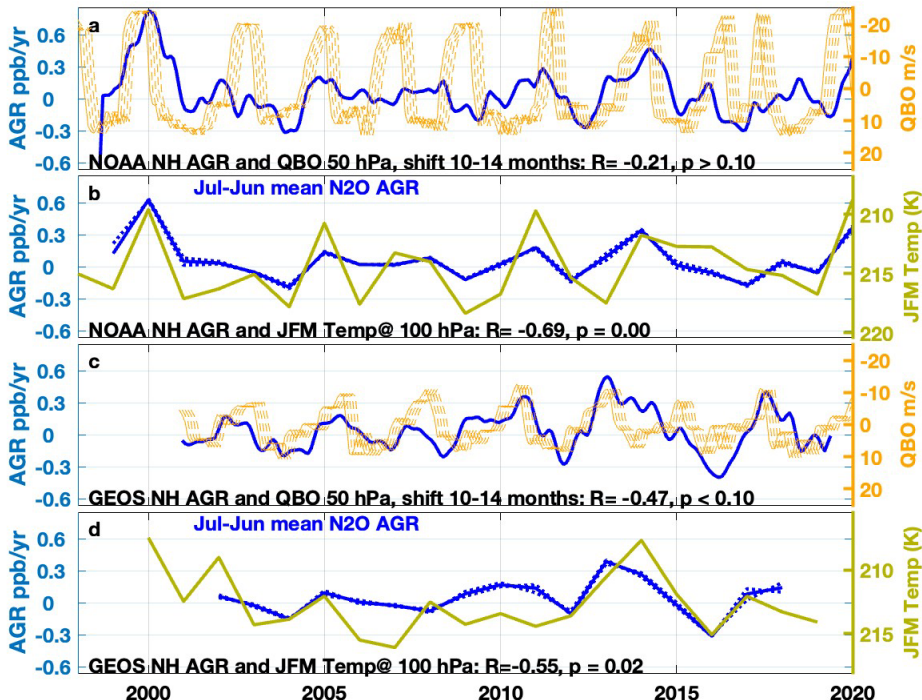
Deleted: A similar

Deleted: is found

Deleted: the GEOSCCM

Deleted: Figure

Deleted: Also in contrast to the SH, the NOAA NH  $N_2O$  AGR is correlated only weakly to the QBO index at all altitudes, with a negative sign. The strongest correlation in the NH occurs for 50 hPa QBO ( $R = -0.23$ ) with a 10-14 months lag (Figure 7a). GEOSCCM predicts a stronger negative correlation ( $R = -0.47$ ) between the GEOSCCM QBO and the NH  $N_2O$  AGR, which also is optimal around 50 hPa with 10-14 month QBO lag (Figure 7c).



Deleted:

635

640

645

Figure 7: NH  $N_2O$  atmospheric growth rate (AGR in ppb/yr) for (a) NOAA and (c) GEOSCCM plotted with the QBO index at 50 hPa with a 10-14 month forward shift in the index. (b,d) NH  $N_2O$  AGR plotted with mean lower stratospheric temperature averaged over 60-90°N for January-March of the year labeled on the X axis. The AGR is averaged from monthly  $N_2O$  data over the encompassing 12 month period July-June (solid blue line), shifted plus or minus 1 month (dotted blue lines), for (b) NOAA and (d) GEOSCCM.

665

Figure 8, which shows correlations between the Niño 3.4 index and the surface N<sub>2</sub>O AGR, shows that that the two are significantly anticorrelated ( $R = -0.4$ ,  $p < 0.05$ ) for both the global and SH N<sub>2</sub>O AGR, with little or no monthly lag in the index. In the NH, the anticorrelation is weaker ( $R = -0.26$ ,  $p > 0.10$ ) with an optimal lag of 7 months in the Niño 3.4 index relative to the NOAA N<sub>2</sub>O AGR (Fig. 8).

- Deleted: T
- Deleted: is
- Deleted: negatively c
- Deleted: =
- Deleted: 5
- Deleted: to the NOAA surface N<sub>2</sub>O AGR
- Deleted: ly and in the
- Deleted: to
- Deleted: 35
- Deleted: Figure

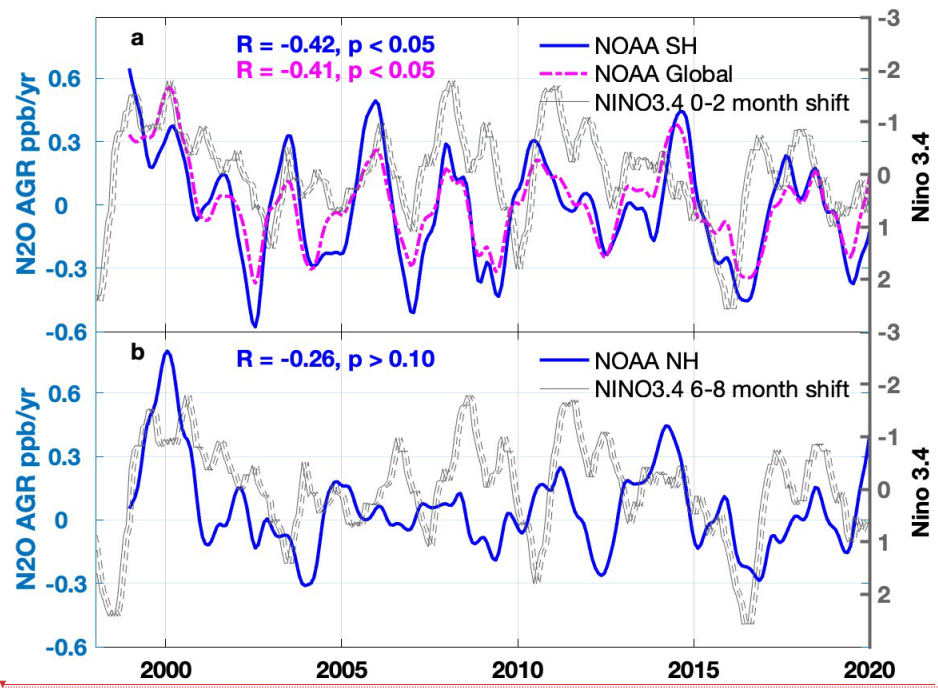
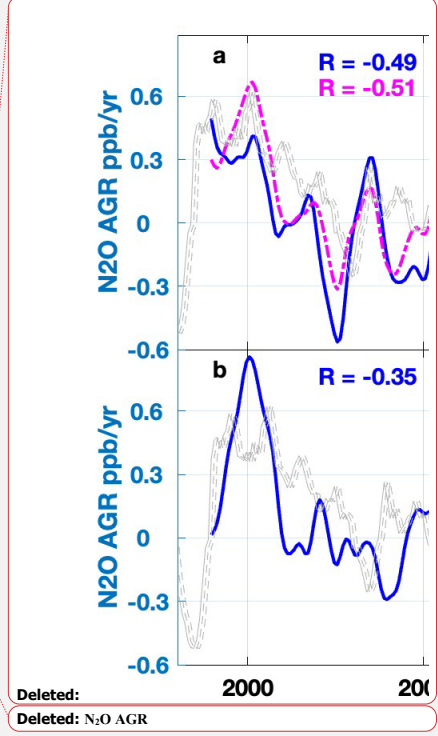


Figure 8: NOAA atmospheric growth rate (AGR in ppb/yr) plotted with the Niño 3.4 index for a) SH and global mean AGR with a 0-2 month shift in the index and b) NH AGR with a 6-8 month shift in the index.

### 670 3.3 Correlation analysis of N<sub>2</sub>O monthly anomalies

The N<sub>2</sub>O monthly anomaly correlation analysis is focused solely on PLST, which has one unique value each year that can be plotted against the corresponding N<sub>2</sub>O anomaly for any given month. The months



- Deleted:
- Deleted: N<sub>2</sub>O AGR

685 selected for this correlation analysis were those surrounding the seasonal N<sub>2</sub>O minimum, which is the most distinct feature of the seasonal cycle [for NOAA sites](#) at remote mid and high latitudes. These months were hypothesized, based on previous work, as most likely to be influenced by the descent of N<sub>2</sub>O-poor air from the stratosphere (Nevison *et al.*, 2011). In contrast, QBO and ENSO are monthly indices for which it is not straightforward to choose a representative month to correlate to the N<sub>2</sub>O monthly anomaly, given that the anomaly might result from the cumulative effect over multiple months.

Figure 9 shows that in the SH, PLST from the previous spring is significantly [anticorrelated](#) to NOAA surface N<sub>2</sub>O monthly anomalies in austral summertime, when N<sub>2</sub>O is descending into its autumn seasonal minimum (Fig. 9a). This correlation [is shown for February at South Pole in Fig. 9b](#) and is observed in [both](#) January and February at several extratropical southern NOAA sites including Cape Grim, Tasmania, Palmer Station, Antarctica, and South Pole. The sign of the correlation is such that more negative surface N<sub>2</sub>O anomalies occur during warm years, in which stronger than average descent of N<sub>2</sub>O-poor air occurs into the polar lower stratosphere over the austral winter and spring. GEOSCCM simulates similar correlations between PLST and austral summer N<sub>2</sub>O anomalies [at these sites](#), both for N<sub>2</sub>O<sub>ST</sub> and total N<sub>2</sub>O [in February](#) (Fig. 9c,d), [and also](#) March, i.e., [the correlations are](#) delayed by about 1 month relative to NOAA surface observations.

Deleted: NOAA sites

Deleted: negatively

Deleted: station

Deleted: Figure

Deleted: and is shown for February at South Pole in Figure 9b

Deleted: Figure

Deleted: at these sites

Deleted: although the correlations are strongest in February and

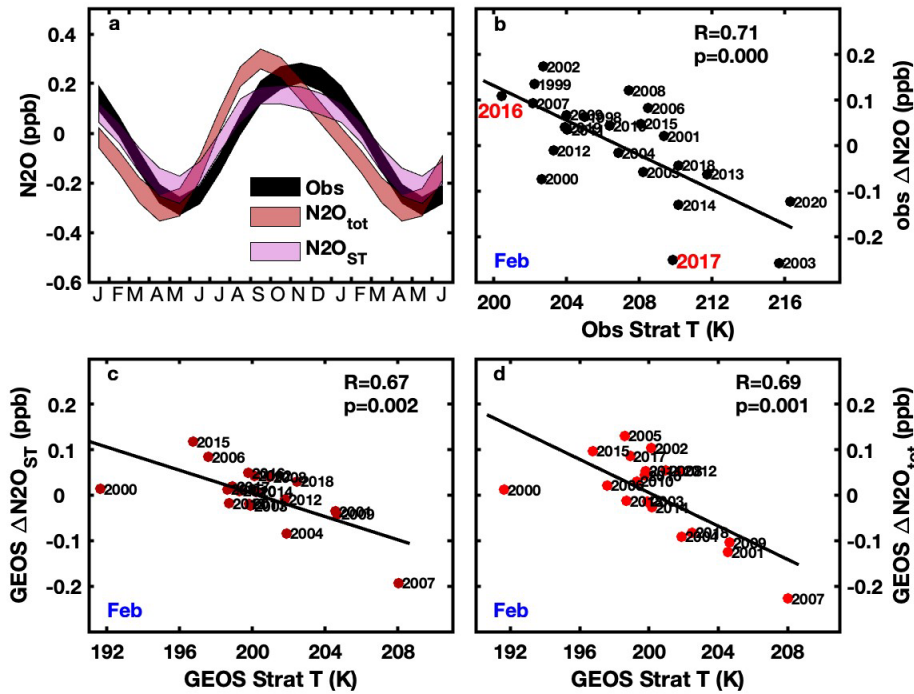
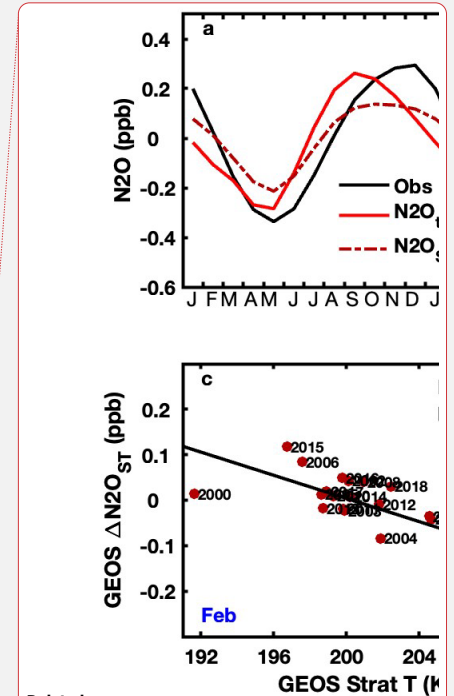


Figure 9: Top row shows a) mean seasonal cycles in  $N_2O$  for NOAA surface station observations (Obs) and GEOSCCM surface total  $N_2O$  ( $N_2O_{tot}$ ) and stratospheric  $N_2O$  ( $N_2O_{ST}$ ) and b) NOAA surface seasonal anomalies of  $N_2O$  mixing ratio (ppb) in February at South Pole spanning 1998-2020, plotted vs. mean lower stratospheric MERRA-2 temperature at 100 hPa averaged over 60-90°S over the previous spring (September-November). The labeled anomalies in 2016 and 2017 correspond to the year of the ORCAS and ATom-2 aircraft surveys, respectively. Bottom row shows GEOSCCM surface seasonal anomalies of  $N_2O$  mixing ratio (ppb) for c)  $N_2O_{ST}$  and d)  $N_2O_{tot}$  in February at South Pole spanning 2000-2019, plotted vs. mean GEOSCCM lower stratospheric temperature, which is sampled the same way as the MERRA-2 temperature.

Figure 10, which compares February altitude-latitude  $N_2O$  contour plots from the ORCAS and ATom airborne surveys, offers some qualitative support for the observed surface correlations in Fig. 9. The contour plots show more depleted  $N_2O$  values in the extratropical SH during ATom-2, which took place in February 2017 after a relatively warm spring in the Antarctic lower stratosphere (strong BDC), compared to ORCAS, which took place in January-February 2016 after a particularly cold spring (weak BDC). The right panel shows ATom-2 data over the full 65°S to 75°N latitude span, putting the



Deleted:

Deleted: South Pole ...ean seasonal cycles ...n  $N_2O$  for ...NOAA surface station observations (Obs) observed  $N_2O$  ...nd ...

Deleted: ... and b) NOAA surface  $N_2O$  ...easonal anomalies of  $N_2O$  mixing ratio (ppb) in February at South Pole spanning 1998-2020, plotted vs. mean lower stratospheric MERRA-2 temperature at 100 hPa averaged over 60-90°S over the previous spring (September-November). The labeled anomalies in 2016 and 2017 correspond to the year of the ORCAS and ATom-2 aircraft surveys, respectively. Bottom row shows GEOSCCM surface GEOSCCM ...

Formatted:

Formatted: Subscript

Deleted: total

Formatted: Subscript

Deleted: Figure

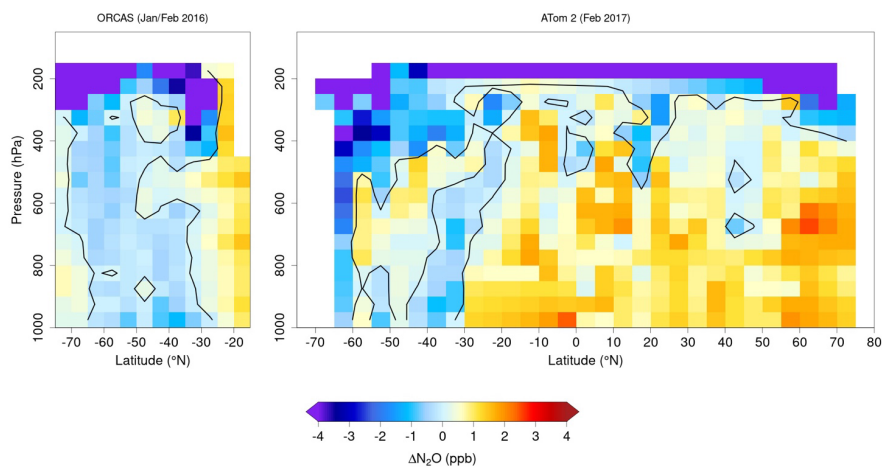
stratospheric influence coming from the southern polar stratosphere into broader perspective. The left panel extends only from 70°S to 20°S because ORCAS was confined to that region. However, the positive anomaly in the mid-troposphere observed at 40-60°S during ATom-2, which may be a source plume from the Southern Ocean, tends to contradict the hypothesis that SH tropospheric N<sub>2</sub>O was lower overall in 2017 than in 2016.

Formatted: Font: Not Bold

Formatted: Font: Not Bold

Formatted: Subscript

Deleted: n.



760 Figure 10. Anomalies of N<sub>2</sub>O in ppb as a function of altitude and latitude from (left panel) ORCAS (Jan.-Feb. 2016) and (right panel) ATom-2 (Jan.-Feb. 2017).

Deleted: anomalies

In contrast to the SH, PLST in the NH from the previous winter is not correlated significantly to N<sub>2</sub>O monthly anomalies at extratropical surface sites for either NOAA or GEOSCCM in any of the months surrounding the NH N<sub>2</sub>O seasonal minimum, with the exception of Mace Head, Ireland, where a negative correlation is found in July in GEOSCCM (Supplementary Fig. S3).

Deleted: NOAA

Deleted:

Deleted: . GEOSCCM also does not predict significant correlations between PLST and summer N<sub>2</sub>O anomalies at most northern NOAA sites...

Deleted: (MHD)

Deleted: Figure

#### 4. Discussion

The atmospheric N<sub>2</sub>O observations and model results assembled here present several new lines of



780 evidence that the stratosphere helps drive the seasonal minimum in tropospheric N<sub>2</sub>O and also  
influences its atmospheric growth rate. First, the vertical cross sections of atmospheric N<sub>2</sub>O from  
aircraft provide a broad-scale perspective, in which N<sub>2</sub>O-poor air enters the winter polar lower  
stratosphere, crosses the tropopause around the time of polar vortex breakup, and descends downward  
and equatorward, reaching Earth's surface by summer or early fall. These patterns are seen in both the  
NOAA empirical background and in global airborne survey data (Fig. 3, 4, 5). Second, GEOSCCM  
785 simulations show similar 3-dimensional patterns to those in the NOAA empirical background (Fig. 4) as  
well as correlations between the surface N<sub>2</sub>O AGR with internally modeled QBO and PLST indices that  
are similar to those found in observations (Fig. 6, 7). In addition, GEOSCCM predicts correlations  
between February N<sub>2</sub>O anomalies and PLST in the SH, both for total N<sub>2</sub>O, similar to those observed,  
and for the tagged stratospheric tracer N<sub>2</sub>O<sub>ST</sub> (Fig. 9).

790 The comparison of GEOSCCM output to NOAA observations, while qualitatively supporting a  
stratospheric influence on the troposphere, also raises questions. The phasing of the GEOSCCM N<sub>2</sub>O  
seasonal cycle is delayed relative to observations, especially in the NH, and the model simulates a too-  
long delay in propagating stratospheric signals down to the surface (Fig. 1,3). Diabatic descent in the  
stratosphere has been shown to be underestimated in atmospheric models (e.g. Brühl et al., 2007;  
795 Khosrawi et al., 2009; 2018) and this may also be the case for air crossing into the troposphere.  
Another issue is that the seasonality of surface N<sub>2</sub>O emissions may not be well represented in the  
GEOSCCM simulation, e.g., summer soil emissions are from a soil biogeochemistry model and may be  
overestimated, leading to unrealistic surface maxima in July (Saikawa et al., 2013; Nevison et al., 2018;  
800 Liang et al., 2022).

With respect to the aircraft data, the NOAA empirical background and QLCS vertical cross sections,  
while showing similar features, are not matched exactly for comparison. QLCS data are measured  
across a narrow longitude band of the flight track for any given latitude on a limited number of days,  
805 while the NOAA empirical background is shown as a monthly mean, zonally averaged across most of  
the western hemisphere (170°-50°W). Consequently, QLCS data are more likely to display synoptic-

Deleted: shows up in

Deleted: ures

Deleted: Figure

Deleted: ures

Deleted: explicitly resolved

Deleted: N<sub>2</sub>O

Deleted: Figure

Deleted:

Deleted: a

Deleted: Figure

Deleted: The rate of

scale variability, such as the apparent surface source plume over the Southern Ocean seen in Fig. 10.

Deleted: s

Deleted: ure

#### 4.1 Correlation to stratospheric indices: signs and magnitudes

820 The results of the correlation analysis based on NOAA surface N<sub>2</sub>O data are similar to those found in  
previous studies based on Advanced Global Atmospheric Gases Experiment (AGAGE) surface N<sub>2</sub>O  
data (Prinn *et al.*, 2000; Nevison *et al.*, 2007; 2011). In general, these correlations are weak, in part  
because the variability in surface N<sub>2</sub>O is very small compared to its mean tropospheric mixing ratio.  
Nevertheless, PLST in the NH correlates significantly to NOAA surface N<sub>2</sub>O AGR anomalies (Fig. 7b)  
825 and PLST in the SH correlates significantly to monthly N<sub>2</sub>O anomalies in February near the time of the  
seasonal N<sub>2</sub>O minimum (Fig. 9b). The negative sign of these correlations is easily understood and  
consistent with more downward transport of N<sub>2</sub>O-poor air and warming of the polar lower stratosphere  
in years with stronger BDC, with subsequent cross-tropopause transport that deepens the descent of  
tropospheric N<sub>2</sub>O into its seasonal minimum and slows the observed AGR of surface N<sub>2</sub>O.

Deleted: Figure

Deleted: Figure

Deleted: warm,

Deleted: into

Deleted: at the surface

830 The reason for the positive correlation of the QBO index with the SH surface N<sub>2</sub>O AGR (Fig. 6a,c) is  
less obvious. A similar correlation in the SH, but not the NH, has been observed in other studies but not  
fully explained (Ray *et al.*, 2020). In our analysis, the positive correlation between the QBO and the SH  
N<sub>2</sub>O AGR is strongest for the QBO at 20 hPa with 17-19 months lag and then weakens with decreasing  
835 QBO altitude down to 100 hPa, with a concurrent decrease in the optimal lag, likely due to the time  
needed for downward propagation of QBO winds (Supplementary Fig. S4). At 50 hPa, we find an  
optimal lag time of 10-12 months ( $R = 0.39$ ), consistent with Ray *et al.* (2020) (who only presented  
results for QBO = 50 hPa).

Deleted: Figure

Deleted: Ray *et al.* (2020)

Deleted: Figure

Deleted: +

Deleted: 3

Deleted: .

840 Photochemical destruction of N<sub>2</sub>O is highest when QBO winds above 30 hPa are in the westerly  
(positive) phase and lower altitude QBO winds are in the easterly (negative) phase. This configuration  
is associated with increased vertical upwelling in the tropical lower stratosphere, which transports more  
N<sub>2</sub>O to its peak loss region around 32 km (Strahan *et al.*, 2021; Ruiz *et al.*, 2021). Thus the magnitude  
of QBO-associated photochemical destruction per se cannot be the main driver of the stratospheric

influence on surface N<sub>2</sub>O, since one would logically expect a negative correlation (i.e., slower growth in the troposphere due to more stratospheric N<sub>2</sub>O loss during positive QBO). *Ruiz et al. (2021)* similarly  
860 concluded that surface variability in N<sub>2</sub>O is not correlated directly to the QBO-driven variability in stratospheric loss, but rather by dynamical variations in cross tropopause fluxes of air, which are governed at least in part by the BDC.

The dynamics of the QBO, its interaction with the BDC and ultimate influence on surface N<sub>2</sub>O are  
865 complex. However, the positive correlation of QBO, peaking at 20 hPa, with the SH N<sub>2</sub>O AGR, could be explained in the context of *Strahan et al. (2015)*, as described in detail in the Supplementary Materials, Section S2. Briefly, the QBO has an associated meridional circulation, which transports N<sub>2</sub>O-poor air poleward from the region of peak photochemical destruction in the tropics between about 30 hPa to 10 hPa in altitude. Paradoxically, this meridional circulation transports less N<sub>2</sub>O-poor air  
870 toward the poles during the phase when the QBO is positive above 30 hPa (i.e., when photochemical destruction is highest). The N<sub>2</sub>O-poor air subsequently is trapped in the Antarctic polar vortex and undergoes BDC-driven diabatic descent, in isolation from mixing with lower latitudes, arriving largely intact in the lower stratosphere and eventually at earth's surface, with a long lag time consistent with the 17-19 month lag found in *Fig. 9a*.

In the NH, the planetary wave activity that drives the BDC is stronger due to the more variable topography and stronger land-sea contrasts. Consequently, the BDC-driven descent into the winter pole is more strongly seasonal and the NH polar vortex is less isolated (*Holton et al., 1995; Scaife and James, 2000; Butchart, 2014; Kidston et al., 2015*), such that any signal associated with the QBO meridional circulation does not transport intact to lower altitudes (*Strahan et al., 2015*). This may  
880 explain why, for both NOAA surface stations and GEOSCCM, the NH N<sub>2</sub>O AGR is more strongly correlated to PLST (a proxy for the BDC) than it is to the QBO, consistent with *Ruiz et al. (2021)*.

Deleted: 1

Deleted: Figure

Deleted: 4.2 Northern vs. southern hemisphere differences

Formatted: Font: Italic

In contrast to the NH, the NOAA SH surface N<sub>2</sub>O AGR does not correlate to PLST. This result is somewhat puzzling given the significant correlation between PLST and NOAA N<sub>2</sub>O February anomalies at SH high latitude surface sites (Fig. 9). It appears that the impact of the stratosphere in austral summer as tropospheric N<sub>2</sub>O descends into its seasonal minimum is not sufficient to influence the N<sub>2</sub>O AGR across the whole SH over the entire year. The SH N<sub>2</sub>O AGR results may reflect the strong preservation of the QBO signal that is ultimately transported into the troposphere, as discussed above, combined with the relatively weaker BDC in the SH and/or the interference of ENSO-driven signals discussed below.

#### 895 4.2 Correlations with ENSO

The NOAA surface station N<sub>2</sub>O AGR correlation with the ENSO index is significant in the SH (R = -0.42, 0-2 month phase shift) but weaker in the NH (R=-0.26, 7 month optimal phase shift) (Fig. 10). The correlation in the SH could in part reflect meteorological shifts in the tropical low level convergence pattern during positive (El Niño) conditions. For atmospheric gases with a positive north-south latitudinal gradient, these shifts result in a lessened influence of winds from the NH on the tropical SH and an increased influence of southeasterly winds. The NOAA Samoa site at 14°S, which strongly influences the cosine-latitude-weighted SH average, is known to be affected by these kinds of wind shifts (Prinn et al., 1992; Nevison et al., 2007). The fact that the N<sub>2</sub>O AGR correlation with ENSO is considerably weaker in the NH than in the SH suggests a limited impact of ENSO on NH N<sub>2</sub>O and supports the hypothesis that reduced north-to-south transport during positive ENSO contributes to the correlation observed in the SH.

The negative correlation between N<sub>2</sub>O AGR and ENSO also may reflect a true reduction in the biogeochemical N<sub>2</sub>O source during the positive ENSO phase, for example, due to drought over tropical land or due to reduced upwelling in the tropical ocean (Ishijima et al., 2009; Thompson et al., 2013). The most well documented biogeochemical response of N<sub>2</sub>O to ENSO events occurs in the Eastern Tropical South Pacific (ETSP), a well known oxygen minimum zone (OMZ) and hot spot of oceanic N<sub>2</sub>O emissions (Arévalo-Martínez, 2015; Ji et al., 2019). El Niño conditions decrease upwelling in the

Deleted: Figure

Deleted: ), which are supported by the ATom-2 and ORCAS data (Figure 10)

Deleted: 3

Deleted: ices

Deleted: similar in magnitude to the correlations with stratospheric indices...

Deleted: 9

Deleted: and relatively

Deleted: 35

Deleted: Figure

Deleted: ENSO

ETSP, thereby reducing the surface productivity, deepening the oxycline, contracting the OMZ and decreasing the N<sub>2</sub>O sea-to-air flux (Ji *et al.*, 2019; Babbin *et al.*, 2015).

930 However, less than one quarter of the total N<sub>2</sub>O budget likely comes from oceanic emissions, of which the ETSP is only one component (Yang *et al.*, 2020; Canadell *et al.*, 2021). This raises questions about whether a reduced ETSP source (or a strengthened source during La Niña periods) has enough leverage to control the overall N<sub>2</sub>O AGR. Ruiz *et al.* (2021) removed the stratospheric influence from surface N<sub>2</sub>O data to infer a source of ~ 1 Tg N (about 5% of the total annual N<sub>2</sub>O source) associated with the 2010 La Niña event, which could have come from tropical land or ocean, or some combination of both. 935 Similarly, Kort *et al.* (2011) found evidence of strong episodic pulses of ~ 1 Tg N from tropical regions, based on maxima in QCLS N<sub>2</sub>O data measured in the middle and upper troposphere during aircraft campaigns in 2009. These pulses were not tied specifically to an ENSO event but rather more generally demonstrated the strength of the tropical N<sub>2</sub>O source.

## 5.2 Summary and Outlook

940 GEOSCCM simulations with a tagged stratospheric tracer show that N<sub>2</sub>O-poor air descends throughout the winter into the polar lower stratosphere, crosses the tropopause in spring or early summer, and descends downward and equatorward, transmitting a diluted but still coherent signal to Earth's surface in late summer to early autumn (August-September in the NH, April-May in the SH). The GEOSCCM simulations are corroborated by N<sub>2</sub>O observations from aircraft, which provide direct evidence for a stratospheric influence on tropospheric N<sub>2</sub>O that previously was inferred primarily based on correlations of surface N<sub>2</sub>O data to stratospheric indices. 945 In support of the model and aircraft results, and consistent with previous studies, significant correlations are found between the N<sub>2</sub>O AGR observed at long-term NOAA surface monitoring sites and either the QBO index in the SH or PLST in the NH, where PLST is a proxy for the strength of the BDC. Correlations between the N<sub>2</sub>O AGR and ENSO indices are also 950 statistically significant in the SH, suggesting a joint influence of ENSO and the stratosphere on the AGR in that hemisphere. The QBO influences the rate at which N<sub>2</sub>O is transported to and destroyed in the tropical stratosphere, but complex atmospheric dynamics buffer how variations in the N<sub>2</sub>O

Deleted: tease out

Deleted: Conclusions

Formatted: Font: Bold

Moved down [5]: N<sub>2</sub>O observations from aircraft provide direct evidence for a stratospheric influence on tropospheric N<sub>2</sub>O that previously was inferred based on correlations of surface N<sub>2</sub>O data to stratospheric indices.

Deleted: corroborate the view

Moved (insertion) [5]

Deleted: this view

Deleted: middle to upper

Deleted: stratospheric

photochemical loss rate are transmitted across the tropopause to modulate the surface N<sub>2</sub>O AGR.

Cross-tropopause transport at high latitudes is linked closely to the BDC and appears to be a more direct influence than the QBO on the N<sub>2</sub>O AGR in the NH. In the SH in contrast, the combination of a better-preserved QBO signal and weaker BDC may lead to a direct (albeit with a ~18 month lag) correlation between the QBO and the SH N<sub>2</sub>O surface AGR, consistent with current knowledge of stratospheric dynamics.

The solar cycle is an additional influence on variability in N<sub>2</sub>O that may be worth investigating in future work. While previous studies have estimated a relatively small effect over the 2000s and 2010s due to low solar activity (Ruiz et al., 2021; Prather et al., 2023), solar cycle-driven changes in the UV flux affect N<sub>2</sub>O photolysis both directly and indirectly through the impact stratospheric O<sub>3</sub>. Another important issue is the impact on N<sub>2</sub>O of climate change driven increases in the strength of the BDC (Garny et al., 2013; Butchart et al., 2014; Fu et al., 2019). Of particular relevance to the results presented here are studies based on ground or satellite based N<sub>2</sub>O observations that find a decrease in the N<sub>2</sub>O lifetime (Prather et al., 2023) and interhemispheric differences in stratospheric N<sub>2</sub>O trends (Minganti et al., 2022). Finally, to help refine our understanding of variability in tropospheric N<sub>2</sub>O, long-term monitoring at surface and aircraft-based sites is essential and would be complemented by more global airborne surveys extending into the lower stratosphere. The latter provide new insights into stratospheric influences on tropospheric N<sub>2</sub>O and advance our ability to interpret and quantify surface N<sub>2</sub>O sources.

#### Code Availability

Codes are available from the corresponding author upon request.

#### 985 Data Availability

NOAA N<sub>2</sub>O data can be obtained by contacting [xin.lan@noaa.gov](mailto:xin.lan@noaa.gov) or through the NOAA Global Monitoring Laboratory at [https://gml.noaa.gov/aftp/data/trace\\_gases/n2o/flask/](https://gml.noaa.gov/aftp/data/trace_gases/n2o/flask/). QCLS N<sub>2</sub>O data are openly available and archived in the Oak Ridge National Laboratory Distributed Active Archive Center (ORNL DAAC) <https://doi.org/10.3334/ORNLDAAC/1925> (ATom), and at the National Center for

**Deleted:** in polar regions

**Deleted:** contrast, in

**Deleted:** 1.5 year

**Deleted:** To further refine our understanding of variability in tropospheric N<sub>2</sub>O, long-term monitoring at surface and aircraft-based sites is essential and would be complemented by more global airborne surveys extending into the lower stratosphere. The latter provide new insights into stratospheric influences on tropospheric N<sub>2</sub>O and advance our ability to interpret and quantify surface N<sub>2</sub>O sources. ...

**Formatted:** Font: Not Bold

**Formatted:** Font: Not Bold

**Formatted:** Font: Not Bold

**Formatted:** Font: Not Bold

**Formatted:** Font: Not Bold

**Deleted:**

**Formatted:** Font: Not Bold

**Formatted:** Font: Not Bold

**Formatted:** Font: Not Bold

Atmospheric Research (NCAR) <https://doi.org/10.5065/D6SB445X> (ORCAS) and [https://doi.org/10.3334/CDIAC/HIPPO\\_010](https://doi.org/10.3334/CDIAC/HIPPO_010) (HIPPO).

#### Author contributions

005 CDN designed and carried out the analysis and prepared the main manuscript and most of the figures. QL implemented separate stratospheric and tropospheric N<sub>2</sub>O tracers in GEOSCCM and provided model output. PN computed QBO indices and MERRA stratospheric temperatures and provided guidance on stratospheric dynamics. BBS, RC, YG and EK provided QCLS N<sub>2</sub>O data and BBS created contour plots of the QCLS data. XL and GD provided N<sub>2</sub>O surface data. All authors reviewed and approved the manuscript.

#### 010 Competing Interests

The authors declare they have no conflicts of interest.

#### Acknowledgments

015 CDN and QL acknowledge support from the NASA MAPS program (award 16-MAP16-0049). The authors are grateful to Arlyn Andrews, Colm Sweeney, Bradley Hall, Ed Dlugokencky, Steve Wofsy, Bruce Daube, and many others who have made this study possible, through collection and analysis of surface station and NOAA aircraft flasks, in situ NOAA station measurements, and QCLS aircraft campaign observations. The HIPPO and ORCAS observations, and the contributions of BBS were supported by the National Center for Atmospheric Research, which is a major facility sponsored by the  
020 [National Science Foundation under Cooperative Agreement No. 1852977. The authors thank Dr. Farahnaz Khosrawi and 2 other anonymous reviewers whose detailed and helpful comments much improved the manuscript.](#)

#### References

- 025 [Akima, H.:](#) A Method of Bivariate Interpolation and Smooth Surface Fitting for Irregularly Distributed Data Points, ACM Transactions on Mathematical Software, Vol. 4, No. 2, June 1978, pp. 148-159. Copyright 1978, Association for Computing Machinery, Inc, 1978
- [Arévalo-Martínez, D. L., Kock, A., Löscher, C. R., Schmitz, R. A. & Bange, H. W.:](#) Massive nitrous oxide emissions from the tropical South Pacific Ocean, *Nat. Geosci.*, 8, 530, 2015.
- [Babbin, A.R., Bianchi, D., Jayakumar, A, and Ward, B. B.:](#) Rapid nitrous oxide cycling in the suboxic ocean, *Science*, 348, doi:10.1126/science.aaa8380, 2015.
- 030 [Baldwin, M.P., Gray, L.J., Dunkerton, T.J., Hamilton, K., Haynes, P.H., Randel, W.J., Holton, J.R., Alexander, M.J., Hirota, I., Horinouchi, T., Jones, D.B.A., Kinnersley, J.S., Marquardt, C., Sato, K., Takahashi, M.:](#) The quasi-biennial oscillation, *Reviews of Geophysics*, 39(2), 179-229, 2001.

Formatted: Font: 12 pt

Formatted: Indent: Left: 0", Hanging: 0.5", Line spacing: single

Deleted: .

Formatted: Indent: Left: 0", Hanging: 0.5"

Deleted: .

- Bouwman, A.F. and Taylor, J.A.: Testing high-resolution nitrous oxide emission estimates against observations using an atmospheric transport model, *Global Biogeochem. Cy.*, 10, 307-318, 1996.
- Bouwman, A.F., van der Hoek, K.W., and Olivier, J.G.J.: Uncertainties in the global source distribution of nitrous oxide, *J. Geophys. Res.*, 100, 2785-2800, 1995.
- Brühl, C., Steil, B., Stiller, G., Funke, B., and Jöckel, P.: Nitrogen compounds and ozone in the stratosphere: comparison of MIPAS satellite data with the chemistry climate model ECHAM5/MESSy1, *Atmos. Chem. Phys.*, 7, 5585-5598, <https://doi.org/10.5194/acp-7-5585-2007>, 2007.
- Butchart, N.: Reviews of Geophysics The Brewer-Dobson *Circulation*, *Rev. Geophys*, 52, 157-184. <https://doi.org/10.1002/2013RG000448>, 2014.
- Canadell, J. G., P. M. S. Monteiro, M. H. Costa, L. Cotrim da Cunha, P. M. Cox, A. V. Eliseev, S. Henson, M. Ishii, S. Jaccard, C. Koven, A. Lohila, P. K. Patra, S. Piao, J. Rogelj, S. Syampungani, S. Zaehle, K. Zickfeld, Global Carbon and other Biogeochemical Cycles and Feedbacks. In: *Climate Change 2021: The Physical Science Basis. Contribution of Working Group I to the Sixth Assessment Report of the Intergovernmental Panel on Climate Change* (Masson-Delmotte, V., P. Zhai, A. Pirani, S. L. Connors, C. Péan, S. Berger, N. Caud, Y. Chen, L. Goldfarb, M. I. Gomis, M. Huang, K. Leitzell, E. Lonnoy, J.B.R. Matthews, T. K. Maycock, T. Waterfield, O. Yelekçi, R. Yu and B. Zhou (eds.)). Cambridge University Press, 2021.
- Earth Systems Research Laboratory, Multivariate ENSO Index (MEI). NOAA (2017).
- Elkins, J.W. and Dutton, G.S.: Nitrous oxide and sulfur hexafluoride (in 'State of the Climate in 2008'), *Bull. Amer. Meteor. Soc.*, 90, S38-S39, 2009.
- Forster, P., Ramaswamy, V., Artaxo, P., Berntsen, T., Betts, R., Fahey, D.W., Haywood, J., Lean, J., Lowe, D.C., Myhre, G., Nganga, J., Prinn, R., Raga, G., Schulz, M. and Van Dorland, R.: Changes in Atmospheric Constituents and in Radiative Forcing. In: *Climate Change 2007: The Physical Science Basis. Contribution of Working Group I to the Fourth Assessment Report of the Intergovernmental Panel on Climate Change*. Cambridge University Press Cambridge, United Kingdom and New York, NY, USA, 2007.
- Fu Q., Solomon S., Pahlavan H.A., Lin P.: Observed changes in Brewer-Dobson circulation for 1980-2018, *Environmental Research Letters*, 14 (11), 114026, DOI: 10.1088/1748-9326/ab4de7, 2019.
- Garny H., Bodeker G.E., Smale D., Dameris M., Grewe V.: Drivers of hemispheric differences in return dates of mid-latitude stratospheric ozone to historical levels, *Atmospheric Chemistry and Physics*, 13 (15), 7279 - 7300, DOI: 10.5194/acp-13-7279-2013, 2013.
- Gonzalez, Y., Commane, R., Manninen, E., Daube, B.C., Schiferl, L., McManus, J.B., McKain, K., Hints, E.J., Elkins, J.W., Montzka, S.A.: Impact of stratospheric air and surface emissions on tropospheric nitrous oxide during ATom, *Atmospheric Chemistry and Physics Discussions*, <https://doi.org/10.5194/acp-2021-167>, 2021.
- Gurney, K. R., Law, R.M., Denning, A.S., Rayner, P.J., Pak, B.C., Baker, D.F., Bousquet, P., Bruhwiler, L., Chen, Y.-H., Ciais, P., Fung, I.Y., Heimann, M., John, J., Maki, T., Maksyutov, S., Peylin, P., Prather, M., Taguchi, S.: Transcom 3 inversion intercomparison: Model mean

Formatted: Font: Times New Roman, 12 pt

Formatted: Indent: Left: 0", Hanging: 0.5", Line spacing: single

Deleted: circulation

Formatted: Indent: Left: 0", Hanging: 0.5"

Deleted: , 2021,

Deleted: . In Press

Formatted: Font: (Default) +Body (Times New Roman), 12 pt

Formatted: Indent: Left: 0", Hanging: 0.5", Space Before: 0 pt, After: 0 pt

Formatted: Font: (Default) +Body (Times New Roman)

Formatted: Font: (Default) +Body (Times New Roman), 12 pt

Formatted: Font: (Default) +Body (Times New Roman)

Formatted: Indent: Left: 0", Hanging: 0.5"

Deleted: ,



results for the estimation of seasonal carbon sources and sinks, *Global Biogeochem. Cycles*, 18, GB1010, doi:10.1029/2003GB002111, 2004.

Hall, B. D., Dutton, G.S., and Elkins, J. W.: The NOAA nitrous oxide standard scale for atmospheric observations, *J. Geophys. Res.*, 112, D09305, doi:10.1029/2006JD007954, 2007.

85 Hall, B. D., Dutton, G. S., Mondeel, D. J., Nance, J. D., Rigby, M., Butler, J. H., Moore, F. L., Hurst, D. F. and Elkins, J. W.: Improving measurements of SF<sub>6</sub> for the study of atmospheric transport and emissions, *Atmos. Meas. Tech.*, 4, 2441-2451, doi: 10.5194/amt-4-2441-2011, 2011.

Hammerling, D. M., Michalak, A. M., Kawa, S. R.: Mapping of CO<sub>2</sub> at High Spatiotemporal Resolution using Satellite Observations: Global Distributions from OCO-2, *Journal of Geophysical Research*, 117, D06306, doi:10.1029/2011JD017015, 2012.

90 Hirsch, A.I., Michalak, A.M., Bruhwiler, L.M., Peters, W., Dlugokencky, E.J. and Tans, P.P.: Inverse modeling estimates of the global nitrous oxide surface flux from 1998-2001, *Global Biogeochem. Cy.*, 20, GB1008, doi:10.1029/2004GB002443, 2006.

95 Holton, J.R., Haynes, P.H., McIntyre, M.E., Douglass, A.R., Rood, R.B. and Pfister, L.: Stratosphere-troposphere exchange. *Rev. Geophys.*, 33(4), 403-439, 1995.

Holton, J.: *An Introduction to Dynamic Meteorology*, no. v. 1 in *An Introduction to Dynamic Meteorology*, Elsevier Science, available at: <https://books.google.be/books?id=fhW5oDv3EPsC>, 2004.

Huang, J., Golombek, A., Prinn, R., Weiss, R., Fraser, P., Simmonds, P., Dlugokencky, E.J., Hall, B., Elkins, J., Steele, P., Langenfelds, R., Krummel, P., Dutton, G., and Porter, L.: Estimation of regional emissions of nitrous oxide from 1997 to 2005 using multinet network measurements, a chemical transport model, and an inverse method, *J. Geophys. Res.*, 113, D17313, doi:10.1029/2007JD009381, 2008.

Ishijima, K., Patra, P.K., Takigawa, M., Machida, T., Matsueda, H., Sawa, Y., Steele, L.P., Krummel, P.B., Langenfelds, R.L., Aoki, S. and Nakazawa, T.: The stratospheric influence on the seasonal cycle of nitrous oxide in the troposphere as deduced from aircraft observations and model simulations, *J. Geophys. Res.*, 115, D20308, doi:10.1029/2009JD013322, 2010.

Ji, Q., Babbin, A.R., Jayakumar, A., Oleyunik, S. and Ward, B.B.: Nitrous oxide production by nitrification and denitrification in the Eastern Tropical South Pacific oxygen minimum zone, *Geophys. Res. Lett.*, 42(24), 10,755–10,764, doi:10.1002/2015gl066853, 2015.

110 Ji, Q. et al.: Investigating the effect of El Niño on nitrous oxide distribution in the eastern tropical South Pacific. *Biogeosciences*, 16(9), 2079–2093, doi:10.5194/bg-16-2079-2019, 2019.

Jiang, X, Ku, W.L., Shia, R.-L., Li, Q., Elkins, J.W., Prinn, R.G., Yung, Y.L.: Seasonal cycle of N<sub>2</sub>O: Analysis of data, *Global Biogeochem. Cy.*, 21, GB1006, doi:10.1029/2006GB002691, 2007.

115 Jin, X. and Gruber, N.: Offsetting the radiative benefit of ocean iron fertilization by enhancing N<sub>2</sub>O emissions, *Geophys. Res. Lett.* 30(24), 2249, 2003.

Jin, X., Najjar, R.G., Louanchi, F., and Doney, S.C.: A modeling study of the seasonal oxygen budget of the global ocean, *J. Geophys. Res.*, 112, C05017, doi:10.1029/2006JC003731, 2007.

120 Kalnay, E., Kanamitsu, M., Kistler, R., Collins, W., Deaven, D., Gandin, L., Iredell, M., Saha, S., White, G., Woollen, J., Zhu, Y., Leetmaa, A., Reynolds, R., Chelliah, M., Ebisuzaki, W., Higgins, W., Janowiak, J., Mo, K.C., Ropelewski, C., Wang, J., Jenne, R., Joseph, D.: The NMC/NCAR 40-year reanalysis project, *B. Am. Meteorol. Soc.*, 77, 437– 471, 1996.

Moved (insertion) [4]

Moved up [4]: Holton, J.R., Haynes, P.H., McIntyre, M.E., Douglass, A.R., Rood, R.B. and Pfister, L.: Stratosphere-troposphere exchange, *Rev. Geophys.*, 33(4), 403-439, 1995.

Formatted: Font: Times New Roman, 12 pt

Deleted: (last access: 28 October 2020)

Formatted: Indent: Left: 0", Hanging: 0.5"

Deleted: 2015:

Deleted: .

Deleted: ical

Deleted: earch

Deleted: ers

- 135 [Khosrawi, F., Müller, R., Proffitt, M. H., Ruhnke, R., Kirner, O., Jöckel, P., Groß, J.-U., Urban, J., Murtagh, D., and Nakajima, H.: Evaluation of CLaMS, KASIMA and ECHAM5/MESSy1 simulations in the lower stratosphere using observations of Odin/SMR and ILAS/ILAS-II. \*Atmos. Chem. Phys.\*, 9, 5759–5783, <https://doi.org/10.5194/acp-9-5759-2009>, 2009.](#)
- 140 [Khosrawi, F., Kirner, O., Stiller, G., Höpfner, M., Santee, M. L., Kellmann, S., and Braesicke, P.: Comparison of ECHAM5/MESSy Atmospheric Chemistry \(EMAC\) simulations of the Arctic winter 2009/2010 and 2010/2011 with Envisat/MIPAS and Aura/MLS observations. \*Atmos. Chem. Phys.\*, 18, 8873–8892, <https://doi.org/10.5194/acp-18-8873-2018>, 2018.](#)
- 140 [Kidston, J., Scaife, A., Hardiman, S. et al.: Stratospheric influence on tropospheric jet streams, storm tracks and surface weather. \*Nature Geosci\* 8, 433–440, <https://doi.org/10.1038/ngeo2424>, 2015.](#)
- 145 [Kort, E. A., Patra, P. K., Ishijima, K., Daube, B. C., Jiménez, R., Elkins, J.W., Hurst, D., Moore, F. L., Sweeney, C. and Wofsy, S. C.: Tropospheric distribution and variability of N<sub>2</sub>O: Evidence for strong tropical emissions. \*Geophys. Res. Lett.\*, 38, L15806, doi:10.1029/2011GL047612, 2011.](#)
- 145 [Kroeze, C., Mosier, A. and Bouwman, L.: Closing the global N<sub>2</sub>O budget: A retrospective analysis 1500–1994, \*Global Biogeochemical Cycles\*, 13, 1–8, 1999.](#)
- 150 [Lambert, A., Read, W. G., Livesey, N. J., Santee, M.L., Manney, G.L., Froidevaux, L., Wu, D.L., Schwartz, M.J., Pumphrey, H.C., Jimenez, C., Nedoluha, G.E., Cofield, R.E., Cuddy, D.T., Daffer, W.H., Drouin, B.J., Fuller, R.A., Jarnot, R.F., Knosp, B.W., Pickett, H.M., Perun, V.S., Snyder, W.V., Stek, P.C., Thurstans, R.P., Wagner, P.A., Waters, J.W., Jucks, K.W., Toon, G.C., Stachnik, R.A., Bernath, P.F., Boone, C.D., Walker, K.A., Urban, J., Murtagh, D., Elkins, J.W., Atlas, E.: Validation of the Aura Microwave Limb Sounder middle atmosphere water vapor and nitrous oxide measurements, \*J. Geophys. Res.\*, 112, D24S36, doi:10.1029/2007JD008724, 2007.](#)
- 155 [Lan, X., Dlugokencky, E.J., Mund, J.W., Crotwell, A.M., Crotwell, M.J., Moglia, E., Madronich, M., Neff, D. and Thoning, K.W.: Atmospheric Nitrous Oxide Dry Air Mole Fractions from the NOAA GML Carbon Cycle Cooperative Global Air Sampling Network, 1997–2021, Version: 2022-11-21, <https://doi.org/10.15138/53g1-x417>, 2022.](#)
- 160 [Lan, X., Tans, P., Thoning, K.: NOAA Global Monitoring Laboratory. NOAA Greenhouse Gas Marine Boundary Layer Reference - N<sub>2</sub>O. \(Data set\). NOAA GML. <https://doi.org/10.15138/83W5-DK71>, 2023.](#)
- 165 [Liang, Q., Stolarski, R.S., Douglass, A.R., Newman, P.A. and Nielsen, J.E.: Evaluation of emissions and transport of CFCs using surface observations and their seasonal cycles and the GEOS CCM simulation with emissions-based forcing, \*J. Geophys. Res.\*, 113, D14302, doi:10.1029/2007JD009617, 2008.](#)
- 170 [Liang, Q., Douglass, A.R., Duncan, B.N., Stolarski, R.S. and Witte, J.C.: The governing processes and timescales of stratosphere-to-troposphere transport and its contribution to ozone in the Arctic troposphere, \*Atmos. Chem. Phys.\*, 9, 3011–3025, 2009.](#)
- [Liang, Q., Nevison, C., Dlugokencky, E., Hall, B. D., & Dutton, G.: 3-D atmospheric modeling of the global budget of N<sub>2</sub>O and its isotopologues for 1980–2019: The impact of anthropogenic emissions. \*Global Biogeochemical Cycles\*, 36, e2021GB007202. <https://doi.org/10.1029/2021GB007202>, 2022.](#)

**Moved down [2]:** Khosrawi, F., Kirner, O., Stiller, G., Höpfner, M., Santee, M. L., Kellmann, S., and Braesicke, P.: Comparison of ECHAM5/MESSy Atmospheric Chemistry (EMAC) simulations of the Arctic winter 2009/2010 and 2010/2011 with Envisat/MIPAS and Aura/MLS observations, *Atmos. Chem. Phys.*, 18, 8873–8892, <https://doi.org/10.5194/acp-18-8873-2018>, 2018.

**Formatted:** Font: (Default) Times New Roman

**Formatted:** Font: Times New Roman, 12 pt

**Formatted:** Indent: Left: 0", Hanging: 0.5", Space Before: 0 pt, After: 0 pt

**Moved (insertion) [2]**

**Deleted:** [Khosrawi, F., Müller, R., Urban, J., Proffitt, M. H., Stiller, G., Kiefer, M., Lossow, S., Kinnison, D., Olschewski, F., Riese, M., and Murtagh, D.: Assessment of the interannual variability and influence of the QBO and upwelling on tracer–tracer distributions of N<sub>2</sub>O and O<sub>3</sub> in the tropical lower stratosphere, \*Atmos. Chem. Phys.\*, 13, 3619–3641, <https://doi.org/10.5194/acp-13-3619-2013>, 2013.](#)

[Khosrawi, F., Müller, R., Urban, J., Proffitt, M. H., Stiller, G., Kiefer, M., Lossow, S., Kinnison, D., Olschewski, F., Riese, M., and Murtagh, D.: Assessment of the interannual variability and influence of the QBO and upwelling on tracer–tracer distributions of N<sub>2</sub>O and O<sub>3</sub> in the tropical lower stratosphere, \*Atmos. Chem. Phys.\*, 13, 3619–3641, <https://doi.org/10.5194/acp-13-3619-2013>, 2013.](#)

**Formatted:** Font: (Default) Times New Roman

**Deleted:**

**Formatted:** Font: Times New Roman, 12 pt

**Formatted:** Indent: Left: 0", Hanging: 0.5", Line spacing: single

**Deleted:** .

**Deleted:** (2015).

**Formatted:** Font: Times New Roman, 12 pt

**Formatted:** Font: Times New Roman, 12 pt

**Formatted:** Indent: Left: 0", Hanging: 0.5"

**Deleted:** -

**Deleted:** ., &

**Deleted:** . (2023).

**Deleted:** .

- Lickley, M., Solomon, S., Kinnison, D., Krummel, P., Mühle, J., O'Doherty, S., et al.: Quantifying the imprints of stratospheric contributions to interhemispheric differences in tropospheric CFC-11, CFC-12, and N<sub>2</sub>O abundances. *Geophys. Res. Lett.*, 48, e2021GL093700. <https://doi.org/10.1029/2021GL093700>, 2021.
- Lovenduski, N.S., Gruber, N., Doney, S.C., and Lima, I.D.: Enhanced CO<sub>2</sub> outgassing in the Southern Ocean from a positive phase of the Southern Annular Mode, *Glob. Biogeochem. Cycles*, 21, GB2026, doi:10.1029/2006GB002900, 2007.
- Lueker, T.J., Walker, S.J., Vollmer, M.K., Keeling, R.F., Nevison, C.D. and Weiss, R.F.: Coastal upwelling air-sea fluxes revealed in atmospheric observations of O<sub>2</sub>/N<sub>2</sub>, CO<sub>2</sub> and N<sub>2</sub>O, *Geophys. Res. Lett.*, 30, 1292, 2003.
- MacFarling Meure, C., Etheridge, D. M., Trudinger, C. M., Steele, L. P., Langenfelds, R. L., van Ommen, T., Smith, A. and Elkins, J. W.: Law Dome CO<sub>2</sub>, CH<sub>4</sub>, and N<sub>2</sub>O ice core records extended to 2000 years BP, *Geophys. Res. Lett.*, 33, L14810, doi:10.1029/2006GL026152, 2006.
- Mahowald, N. M., Rasch, P. J., Eaton, B. E., Whittlestone, S. and Prinn, R. G.: Transport of radon-222 to the remote troposphere using the Model of Atmospheric Transport and Chemistry and assimilated winds from ECMWF and the National Center for Environmental Prediction/NCAR, *J. Geophys. Res.*, 102, 28139–28151, 1997.
- Masarie, K. A. and Tans, P.P.: Extension and integration of atmospheric carbon dioxide data into a globally consistent measurement record, *Journal of Geophysical Research-Atmospheres*, 100, D6, 11593-11610, 1995.
- McPhaden, M. J., et al.: The tropical ocean-global atmosphere observing system: A decade of progress, *J. Geophys. Res.*, 103, 14,169–14,240, doi:10.1029/97JC02906, 1998.
- Minganti, D., Chabrilat, S., Christophe, Y., Errera, Q., Abalos, M., Prignon, M., Kinnison, D. E., and Mahieu, E.: Climatological impact of the Brewer–Dobson **Circulation** on the N<sub>2</sub>O budget in WACCM, a chemical reanalysis and a CTM driven by four dynamical reanalyses, *Atmos. Chem. Phys.*, 20, 12609–12631, <https://doi.org/10.5194/acp-20-12609-2020>, 2020.
- Minganti, D., Chabrilat, S., Errera, Q., Prignon, M., Kinnison, D. E., Garcia, R. R., et al.: Evaluation of the N<sub>2</sub>O rate of change to understand the stratospheric Brewer-Dobson **Circulation** in a Chemistry-Climate Model. *Journal of Geophysical Research: Atmospheres*, 127, e2021JD036390. <https://doi.org/10.1029/2021JD036390>, 2022.
- Mosier, A.R., Duxbury, J.M., Frenay, J.R., Heinemeyer, O. and Minami, K.: Assessing and mitigating N<sub>2</sub>O emissions from agricultural soils, *Climatic Change*, 40, 7-38, 2000.
- Naqvi, S.W.A., Jayakumar, D.A., Narvekar, P.V., Naik, H., Sarma, V.V.S.S., D'Sousa, W., Joseph, S., and George, M.D.: Increased marine production of N<sub>2</sub>O due to intensifying anoxia on the Indian continental shelf, *Nature*, 408, 346-349, 2000.
- Nash, E.R., Newman, P.A., Rosenfield, J.E., and Schoeberl, M.R.: An objective determination of the polar vortex using Ertel's potential vorticity, *J. Geophys. Res.*, 101, 9471-9478, 1996.
- National Oceanic Atmospheric Administration (NOAA) Global Monitoring Division, Interactive Data Visualization, <https://www.esrl.noaa.gov/gmd/dv/iadv/>, accessed April 6, 2021.
- Nevison, C.D., Weiss, R.F. and Erickson III, D.J.: Global Oceanic Nitrous Oxide Emissions, *J. Geophys. Res.*, 100, 15,809-15,820, 1995.

**Deleted:** ical

**Deleted:** earch

**Deleted:** ers

**Deleted:**

**Formatted:** Font: 12 pt

**Formatted:** Indent: Left: 0", Hanging: 0.5", Line spacing: single

**Formatted:** Indent: Left: 0", Hanging: 0.5"

**Formatted:** Font: Times New Roman, 12 pt

**Formatted:** Indent: Left: 0", Hanging: 0.5", Line spacing: single

**Deleted:** circulation

**Deleted:** (2022).

**Deleted:** circulation

**Formatted:** Font: Times New Roman, 12 pt

**Formatted:** Font: Times New Roman, 12 pt

**Formatted:** Font: 12 pt

**Formatted:** Indent: Left: 0", Hanging: 0.5"

- Nevison, C.D., Kinnison, D.E. and Weiss, R.F.: Stratospheric Influence on the tropospheric seasonal cycles of nitrous oxide and chlorofluorocarbons, *Geophys. Res. Lett.* 31(20), L20103, doi:10.1029/2004GL020398, 2004.
- Nevison, C.D., Keeling, R.F., Weiss, R.F., Popp, B.N., Jin, X., Fraser, P.J, Porter, L.W. and Hess, P.G.: Southern Ocean ventilation inferred from seasonal cycles of atmospheric N<sub>2</sub>O and O<sub>2</sub>/N<sub>2</sub> at Cape Grim, Tasmania, *Tellus*, 57B, 218-229, 2005.
- Nevison, C. D., Mahowald, N. M., Weiss, R.F. and Prinn, R.G.: Interannual and seasonal variability in atmospheric N<sub>2</sub>O, *Global Biogeochem. Cy.*, 21, GB3017, doi:10.1029/2006GB002755, 2007.
- Nevison, C.D., Dlugokencky, E., Dutton, G., Elkins, J.W., Fraser, P., Hall, B., Krummel, P.B., Langenfelds, R.L., O'Doherty, S., Prinn, R.G., Steele, L.P., Weiss, R.F.: Exploring causes of interannual variability in the seasonal cycles of tropospheric nitrous oxide, *Atmospheric Chemistry and Physics*, 11, doi:10.5194/acp-11-1-2011, 1-18, 2011.
- Nevison, C., Andrews, A., Thoning, K., Dlugokencky, E., Sweeney, C., Miller, S., et al.: Nitrous oxide emissions estimated with the CarbonTracker-Lagrange North American regional inversion framework. *Global Biogeochemical Cycles*, 32. <https://doi.org/10.1002/2017GB005759>, 2018.
- Newman, P.: The Quasi-biennial Oscillation (QBO). Retrieved from [https://acd-ext.gsfc.nasa.gov/Data\\_services/met/qbo/qbo.html](https://acd-ext.gsfc.nasa.gov/Data_services/met/qbo/qbo.html), 2020.
- Nielsen, J.E., Pawson, S., Molod, A., Auer, B., da Silva, A.M., Douglass, A.R., et al.: Chemical mechanisms and their applications in the Goddard Earth Observing System (GEOS) Earth system model, *Journal of Advances in Modeling Earth Systems*, 9(8), 3019-3044, doi:10.1002/2017MS001011, 2017.
- Olivier, J.G.J., Van Aardenne, J.A., Dentener, F., Ganzeveld, L. and Peters, W.: Recent trends in global greenhouse gas emissions: regional trends and spatial distribution of key sources. In: *Non-CO<sub>2</sub> Greenhouse Gases (NCGG-4)*, van Amstel, A. (coord.), page 325-330. Millpress, Rotterdam, 2005.
- Park, S., et al.: Trends and seasonal cycles in the isotopic composition of nitrous oxide since 1940, *Nature Geoscience*, 5, 261-265, 2012.
- Plumb, R. A.: Stratospheric transport, *J. Meteorol. Soc. Jpn.*, 80, 793-809, 2002.
- Prather, M. Hsu, J., DeLuca, N.M., Jackman, C.H., Oman, L.D., Douglass, A.R., Fleming, E.L., Strahan, S.E., Steenrod, S.D., Sovde, O.A., Isaksen, I.S.A., Froidevaux, L., Funke, B.: Measuring and modeling the lifetime of nitrous oxide including its variability, *J. Geophys. Res. Atmos.*, 120, doi:10.1002/2015JD023267, 2015.
- Prinn, R.G., Weiss, R.F., Fraser, P.J., Simmonds, P.G., Cunnold, D.M., Alyea, F.N., O'Doherty, S., Salameh, P., Miller, B.R., Huang, J., Wang, R.H.J., Hartley, D.E., Harth, C., Steele, L.P., Sturrock, G., Midgley, P.M. and McCulloch, A.: A history of chemically and radiatively important gases in air deduced from ALE/GAGE/AGAGE, *J. Geophys. Res.*, 105 (D14), 17751-17792, 2000.
- Ravishankara A. R., Daniel, J. S. and Portmann, R. W.: Nitrous Oxide (N<sub>2</sub>O): The dominant ozone depleting substance emitted in the 21st century, *Science*, 326, 123-125, doi: 10.1126/science.1176985, 2009.

Formatted: Font: 12 pt

Formatted: Indent: Left: 0", Hanging: 0.5", Line spacing: single

Formatted: Indent: Left: 0", Hanging: 0.5"

- Ray, E. A., Portmann, R. W., Yu, P., Daniel, J., Montzka, S. A., Dutton, G. S., et al.: The influence of the stratospheric Quasi-Biennial Oscillation on trace gas levels at the Earth's surface, *Nature Geoscience*, 13(1), 22–27. <https://doi.org/10.1038/s41561-019-0507-3>, 2020.
- Ruiz, D.J., Prather, M.J., Strahan, S.E., Thompson, R.L., Froidevaux, L., and Steenrod, S.D.: How atmospheric chemistry and transport drive surface variability of N<sub>2</sub>O and CFC-11, *J. Geophys. Res.*, 2021.
- Saikawa, E., Schlosser, C.A. and Prinn, R.G.: Global modeling of soil nitrous oxide emissions from natural processes, *Glob. Biogeochem. Cyc.*, 27, doi:10.1002/gbc.20087, 2013.
- Santoni, G. W., Daube, B. C., Kort, E. A., Jiménez, R., Park, S., Pittman, J. V., Gottlieb, E., Xiang, B., Zahniser, M. S., Nelson, D. D., McManus, J. B., Peischl, J., Ryerson, T. B., Holloway, J. S., Andrews, A. E., Sweeney, C., Hall, B., Hints, E. J., Moore, F. L., Elkins, J. W., Hurst, D. F., Stephens, B. B., Bent, J., and Wofsy, S. C.: Evaluation of the airborne quantum cascade laser spectrometer (QCLS) measurements of the carbon and greenhouse gas suite – CO<sub>2</sub>, CH<sub>4</sub>, N<sub>2</sub>O, and CO – during the CalNex and HIPPO campaigns, *Atmos. Meas. Tech.*, 7, 1509–1526, <https://doi.org/10.5194/amt-7-1509-2014>, 2014.
- Scaife, A.A. and James, I.N.: Response of the stratosphere to interannual variability of tropospheric planetary waves, *Q.J.R. Meteorol. Soc.*, 126: 275– 297. <https://doi.org/10.1002/qj.49712656214>, 2000.
- Shepherd, T. G.: *Transport in the middle atmosphere. J. Meteorol. Soc. Jpn. Ser. II*, 85, 165–191, 2007.
- Sokal, R.R. and Rohlf, F.J.: *Biometry*, 859 pp., W.H. Freeman, New York, 1981.
- Stephens, B.: ORCAS Merge Products. Version 1.0, <https://doi.org/10.5065/D6SB445X>, accessed 13 Jul 2020, 2017.
- Stephens, B. B., Long, M. C., Keeling, R. F., Kort, E. A., Sweeney, C., Apel, E. C., Atlas, E. L., Beaton, S., Bent, J. D., Blake, N. J., Bresch, J. F., Casey, J., Daube, B. C., Diao, M., Diaz, E., Dierssen, H., Donets, V., Gao, B.-C., Gierach, M., Green, R., Haag, J., Hayman, M., Hills, A. J., Hoecker-Martínez, M. S., Honomichl, S. B., Hornbrook, R. S., Jensen, J. B., Li, R.-R., McCubbin, I., McKain, K., Morgan, E. J., Nolte, S., Powers, J. G., Rainwater, B., Randolph, K., Reeves, M., Schauffler, S. M., Smith, K., Smith, M., Stith, J., Stossmeister, G., Toohey, D. W., and Watt, A. S.: The O<sub>2</sub>/N<sub>2</sub> Ratio and CO<sub>2</sub> Airborne Southern Ocean Study, *B. Am. Meteorol. Soc.*, 99, 381–402, <https://doi.org/10.1175/BAMS-D-16-0206.1>, 2018.
- Stohl, A.: A 1-year Lagrangian “climatology” of airstreams in the Northern Hemisphere troposphere and lowermost stratosphere, *J. Geophys. Res.*, 106(D7), 7263–7279, 2001.
- Strahan, S. E., Oman, L.D., Douglass, A.R. and Coy, L.: Modulation of Antarctic vortex composition by the quasi-biennial oscillation, *Geophys. Res. Lett.*, 42, 4216–4223, doi:10.1002/2015GL063759, 2015.
- Thompson, R.L., Dlugokencky, E., Chevallier, F., Ciais, P., Dutton, G., Langenfelds, R.L., Prinn, R.G., Weiss, R.F., Tohjima, Y., O’Doherty, S., Krummel, P.B., Fraser, P., and Steele, L.P.: Interannual variability in tropospheric nitrous oxide, 2013, *Geophys. Res. Lett.*, 40, 4426–4431, doi:10.1002/grl.50721, 2013.
- Thompson, R. L., Patra, P. K., Ishijima, K., Saikawa, E., Corazza, M., Karstens, U., et al.: TransCom N<sub>2</sub>O model inter-comparison-Part 1: Assessing the influence of transport and surface fluxes on

Deleted: .

Formatted: Justified, Indent Left: 0", Hanging: 0.5", Tab stops: Not at 0.39" + 0.78" + 1.17" + 1.56" + 1.94" + 2.33" + 2.72" + 3.11" + 3.5" + 3.89" + 4.28" + 4.67"

Formatted: Font: Not Italic

Formatted: Font: Not Italic

Formatted: Font: Not Italic

Formatted: Font: Not Italic

Formatted: Font color: Gray-85%

Formatted: Indent Left: 0", Hanging: 0.5"

Deleted: Sokal, R.R. and Rohlf, F.J.: *Biometry*, 859 pp., W.H. Freeman, New York, 1981.

Deleted: (2000),

Deleted: .

Deleted: .

Formatted: Font: 12 pt

Deleted: .

Moved (insertion) [3]

Formatted: Font color: Text 1

Formatted: Header, Space Before: 0 pt, After: 0 pt, Tab stops: 4", Left

Formatted: Font: 12 pt

Formatted: Indent Left: 0", Hanging: 0.5", Line spacing: single

Formatted: Font: 12 pt

Formatted: Font: 12 pt

Formatted: Font: 12 pt

Moved up [3]: Shepherd, T. G.: *Transport in the middle atmosphere, J. Meteorol. Soc. Jpn. Ser. II*, 85, 165–191, 2007.

Deleted: Tian, H., Xu, R., Canadell, J.G. et al. A comprehensive quantification of global nitrous oxide sources and sinks. *Nature* 586, 248–256 (2020).

Deleted: -

- 345 tropospheric N<sub>2</sub>O variability, *Atmospheric Chemistry and Physics*, 14(8), 4349–4368.  
<https://doi.org/10.5194/acp-14-4349-2014>, 2014a.
- 350 Thompson, R. L., Ishijima, K., Saikawa, E., Corazza, M., Karstens, U., Patra, P. K., Bergamaschi, P.,  
Chevallier, F., Dlugokencky, E., Prinn, R. G., Weiss, R. F., O’Doherty, S., Fraser, P. J., Steele,  
L. P., Krummel, P. B., Vermeulen, A., Tohjima, Y., Jordan, A., Haszpra, L., Steinbacher, M.,  
Van der Laan, S., Aalto, T., Meinhardt, F., Popa, M. E., Moncrieff, J., and P. Bousquet:  
TransCom N<sub>2</sub>O model inter-comparison, Part II: Atmospheric inversion estimates of N<sub>2</sub>O  
emissions, *Atmos. Chem. Phys. Discuss.*, 14, 5271–5321, doi:10.5194/acpd-14-5271-2014,  
2014b.
- 355 Thompson, R.L., Lassaletta, L., Patra, P.K., Wilson, C., Wells, K.C., Gressent, A., Koffi, E.N.,  
Chipperfield, M.P., Winiwarter, W., Davidson, E.A., Tian, H. and Canadell, J.G.: Acceleration  
of global N<sub>2</sub>O emissions seen from two decades of atmospheric inversion, *Nature Climate  
Change*, <https://doi.org/10.1038/s41558-019-0613-7>, 2019.
- 360 Thompson, T.M., Elkins, J.W., Hall, B., Dutton, G.S., Swanson, T.H., Butler, J.H., Cummings, S.O.,  
Fisher, D.A.: Halocarbons and other Atmospheric Trace Species, in: Schnell, R.C., A.-M.  
Buggle and R.M. Rosson (Eds.), *Climate Diagnostics Laboratory Summary Report #27, 2002-  
2003*, US Department of Commerce, National Oceanic and Atmospheric Administration,  
Boulder, Colorado, 2004.
- 365 Thompson, C.R., Wofsy, S.C., Prather, M.J., Newman, P.A., Hanisco, T.F., Ryerson, T.B., Fahey,  
D.W., Apel, E.C., Brock, C.A., Brune, W.H. et al.: The NASA Atmospheric Tomography  
(ATom) mission: Imaging the chemistry of the global atmosphere, *Bulletin of the American  
Meteorological Society*, 103 (3): E761–E790. DOI: <http://dx.doi.org/10.1175/bams-d-20-0315.1>,  
2022.
- 370 Tian, H., Xu, R., Canadell, J.G., Thompson, R.L., Winiwarter, W., Suntharalingam, P., Davidson, E.A.,  
Ciais, P., et al.: A comprehensive quantification of global nitrous oxide sources and sinks,  
*Nature*, 586, 248-255. <https://doi.org/10.1038/s41586-020-2780-0>, 2020.
- Volk, C.M., Elkins, J.W., Fahey, D., Dutton, G., Gilligan, J., Lowenstein, M., Podolske, J., Chan, K.,  
and Gunson, M.: Evaluation of source gas lifetimes from stratospheric observations, *J. Geophys.  
Res.*, 102(D21), 25,543-25,564, 1997.
- 375 Waugh, D.W., Randel, W.J., Pawson, S., Newman, P.A. and Nash, E.R.: Persistence of the lower  
stratospheric polar vortices, *J. Geophys. Res.*, 104 (D22), 27,191-27,201, 1999.
- Weiss, R.F.: The temporal and spatial distribution of tropospheric nitrous oxide, *J. Geophys. Res.* 86,  
7185-7195, 1981.
- 380 Wofsy, S. C., the HIPPO Science Team and Cooperating Modellers and Satellite Teams: HIAPER Pole-  
to-Pole Observations (HIPPO): Fine grained, global scale measurements for determining rates  
for transport, surface emissions, and removal of climatically important atmospheric gases and  
aerosols, *Phil. Trans. of the Royal Society A*, 369(1943), doi:10.1098/rsta.2010.0313, 2073-  
2086, 2011.
- 385 Wofsy, S., Afshar, S., Allen, H., Apel, E., Asher, E., Barletta, B., Bent, J., Bian, H., Biggs, B., Blake,  
D., and et al.: ATom: Merged Atmospheric Chemistry, Trace Gases, and Aerosols,  
<https://doi.org/10.3334/ORNLDAAAC/1581>, accessed 13 Jul 2020, 2018.
- Wofsy, S., Daube, B., Jimenez, R., Kort, E., Pittman, J., Park, S., Commane, R., Xiang, B., Santoni, G.,

Deleted: a

Deleted: .

Formatted: Font: (Default) Times New Roman, 12 pt

Formatted: Indent: Left: 0", Hanging: 0.5", Line spacing: single

Formatted: Indent: Left: 0", Hanging: 0.5"

Deleted: ¶

Formatted: Font: 12 pt

Formatted: Font: Times New Roman, 12 pt

Formatted: Font: 12 pt

Formatted: Indent: Left: 0", Hanging: 0.5"

Formatted: Font: 12 pt

Formatted: Indent: Left: 0", Hanging: 0.5", Line spacing: single

Formatted: Indent: Left: 0", Hanging: 0.5"

- 390 Jacob, D., and et al.: HIPPO Merged 10-Second Meteorology, Atmospheric Chemistry, and  
Aerosol Data. Version 1.0, [https://doi.org/10.3334/CDIAC/HIPPO\\_010](https://doi.org/10.3334/CDIAC/HIPPO_010), accessed 13 Jul 2020,  
2017.
- | WMO Greenhouse Gas Bulletin No. 14, [https://library.wmo.int/doc\\_num.php?explnum\\_id=5455](https://library.wmo.int/doc_num.php?explnum_id=5455),  
2018.
- β95 Yang, S. et al.: Global reconstruction reduces the uncertainty of oceanic nitrous oxide emissions and  
reveals a vigorous seasonal cycle, *Proceedings of the National Academy of Sciences*, 117(22),  
11954–11960, doi:10.1073/pnas.1921914117, 2020.

Page 23: [1] Deleted Cynthia Nevison 7/9/24 1:22:00 PM

Page 23: [1] Deleted Cynthia Nevison 7/9/24 1:22:00 PM

Page 23: [1] Deleted Cynthia Nevison 7/9/24 1:22:00 PM

Page 23: [1] Deleted Cynthia Nevison 7/9/24 1:22:00 PM

Page 23: [1] Deleted Cynthia Nevison 7/9/24 1:22:00 PM

Page 23: [2] Formatted Cynthia Nevison 7/9/24 1:24:00 PM

Subscript

Page 23: [2] Formatted Cynthia Nevison 7/9/24 1:24:00 PM

Subscript

Page 23: [2] Formatted Cynthia Nevison 7/9/24 1:24:00 PM

Subscript

Page 23: [3] Deleted Cynthia Nevison 7/9/24 1:23:00 PM

Page 23: [3] Deleted Cynthia Nevison 7/9/24 1:23:00 PM

Page 23: [3] Deleted Cynthia Nevison 7/9/24 1:23:00 PM